Evaluation of Machine Learning Algorithms for Modeling Therapist Assistance during Gait Rehabilitation

by

Mason Smith

A Thesis Presented in Partial Fulfillment
Of the Requirements for the Degree
Master of Science

Approved April 2021 by the
Graduate Supervisory Committee:

Wenlong Zhang, Chair
Hani Ben Amor
Thomas Sugar

ARIZONA STATE UNIVERSITY

May 2021

ABSTRACT

Robotic assisted devices in gait rehabilitation have not seen penetration into clinical settings proportionate to the developments in this field. A possible reason for this is due to the development and evaluation of these devices from a predominantly engineering perspective. One way to mitigate this effect is to further include the principles of neurophysiology into the development of these systems. To further include these principles, this research proposes a method for grounded evaluation of three machine learning algorithms to gain insight on what modeling approaches are able to both replicate therapist assistance and emulate therapist strategies. The algorithms evaluated in this paper include ordinary least squares regression (OLS), gaussian process regression (GPR) and inverse reinforcement learning (IRL). The results show that grounded evaluation is able to provide evidence to support the algorithms at a higher resolution. Also, it was observed that GPR is likely the most accurate algorithm to replicate therapist assistance and to emulate therapist adaptation strategies.

ACKNOWLEDGMENTS

This research would like to acknowledge the members of ASU RISE Labs for the feedback and input that was provided throughout the course of this project. Particularly, Seyed Mostafa Rezayat was actively helpful as a professional and academic resource throughout the entire course of this project. I would also like to give a special thanks to my thesis chair, Dr. Wenlong Zhang, for the constant feedback and motivation to continue to push the results of this research to its current state.

TABLE OF CONTENTS

CHAPTER Page

LIST OF TABLES

Table Page

LIST OF FIGURES

Figure Page

Figure Page

1. INTRODUCTION

A. Background

Strokes are currently among the leading causes of prolonged disability in America. It is estimated that over 6.6 million Americans suffer a stroke annually and projections show that this number will increase by 3.4 million by 2030 [1]. Victims who suffer from this acute condition often develop another condition known as hemiparesis. Hemiparesis is the impairment of one side of the body that manifests as muscular weakness, spasticity, or loss of motor control in a limb. [2] Consequently, affected individuals may not be able to live independently due to their inability to perform activities of daily living (ADLs) like walking or feeding themselves. Although it is possible to regain motor function that was lost due to a stroke, this process is complex and requires numerous hours of intense physical therapy.

To understand the process of gait rehabilitation, it is first important to obtain a basic understanding of neurophysiology as it pertains to regaining motor function for patients who have deficits. The process of walking involves complex interactions between the spinal cord and brain. The former is capable of generating simple patterns of locomotion while the latter provides fine motor control, voluntary changes to the gait pattern and processing of sensory feedback to adapt to the requirements of the environment. Post-stroke patients exhibit impairment to areas of the brain like the motor cortex, cerebellum, and brain stem while the spinal cord remains intact [3]. This means that the spinal cord can be used to reorganize the cortex for walking by providing the appropriate proprioceptive input during the task. This is the underlying concept behind

the traditional, bottom-up approach to rehabilitation therapy that uses the mechanics of neural plasticity to help patients overcome their deficits through high dose and high intensity rehabilitation [4].

Generally, early and intense rehabilitation is shown to benefit patient's ability to perform a task like walking [5]. All rehabilitation approaches progress, depending on the level of impairment, through stages of preparatory exercises, direct manipulation of the limb by a therapist over a regular surface and assisted walking over ground. The principles of neurological gait rehabilitation that are seen throughout all of these stages can be classified as either neurophysiological or motor learning techniques [4].

Neurophysiological techniques refer to providing a sensory input or stimulus in order to facilitate voluntary movement. This is typically done by a therapist facilitating the correct movement patterns while the patient remains passive [6]. Many different methods within this approach have been proposed to address muscle spasticity through passive mobilization, reflex stimulation, peripheral sensory inputs [4] but, for the purposes of the research, we will mainly focus on motor learning techniques.

In contrast to the neurophysiological approach, motor learning stresses active engagement in the exercises which is critical for the patient's recovery of motor function. Typically these exercises are done with the context of a the functional task that is being trained [4]. Assisted overground walking (AOW) is one example of a functional task. During AOW, a patient is instructed to walk while therapists provide weight support and movement assistance to stimulate the correct proprioceptive input. Furthermore, assisted overground walking is the rehabilitation context that this paper is investigating.

Even though there are several strategies for improving rehabilitation outcomes, conventional gait therapy typically does not allow stroke patients to recover their full normal gait pattern. A possible cause of this is that the neurophysiological mechanisms involved in recovering motor function is largely unknown. Consequently, there are still many open questions in the field of gait rehabilitation. Answers to these questions could have significant impacts on how rehabilitation is conducted. This, coupled with the potential implications on the quality of living for an increasing population of post-stroke patients', makes for an active field of research. The subset of this field that this paper will be addressing is assistive robotic devices in assisted overground rehabilitation. Research contributions of robotic devices to the field of rehabilitation is unique because these devices can address issues that would otherwise be challenging through conventional therapy methods.

One of the core challenges addressed by these devices is the accessibility of patients to occupational therapists. Accessibility mainly limits the therapy dosage which is widely considered to have a strong correlation with positive patient outcomes. An issue that is contributing to this challenge is that assisted overground walking usually requires at least two therapists; one to support the weight of the patient and the other to assist in providing the correct proprioceptive input for the patient's leg. Robotic aids may provide a means to decrease the number of therapists needed per patient and reduce the manhours for an individual patient's session. As a consequence, these devices have the potential to increase the availability of therapists at any given time and decrease healthcare costs [4] which can improve accessibility to low-income patients.

Another challenge with assisted overground walking is that it can quickly cause therapists to fatigue. To provide proper assistance, therapists are often put in uncomfortable positions for extended periods of time. This has the potential to limit the duration of a patient's rehabilitation session due to fatigue of the therapist even though the patient could potentially continue. Consequently, therapist fatigue may limit the intensity and dosage of therapy sessions due to the physical demands and required therapist rest between sessions. Robotic aids address this challenge by reducing the strain of this labor-intensive task. This can be done by removing therapists from these positions with poor ergonomics and reducing physical actuation from a therapist [7]. Addressing therapist fatigue is significant since it will mitigate the mentioned limitations placed on both dosage and intensity.

Robotic aids also bring a few novel benefits over conventional therapy. First, a robotic device is able to provide a more precise and consistent assistance due to the mechanical and quantifiable nature of the device. This has the potential to allow future robotic devices to provide a rehabilitation process that is more repeatable and specifically tuned to patient needs. Secondly, a robotic platform is able to measure quantifiable patient statistics like performance and motor impairment characteristics that can provide a better insight than current clinical scales [8,9].

B. Problem Statement

The current body of literature surrounding the field of robot assisted rehabilitation is rapidly progressing and advances to current wearable devices are being developed at an increasing rate. However, the penetration of these devices into practical clinical settings is disproportionate to the advancements made in the field. A suspected source of this

disparity is due to much of the current volume of research approaching this field from a perspective highly focused on engineering-design instead of a clinical perspective grounded in the principles of occupational therapy [10]. Approaching the problem of modeling therapist interaction from a predominantly engineer perspective can cause a biased design and evaluation of a model. This can present itself in the form of explicitly optimizing the system to replicate the data observed during a rehabilitation session.

Although this criterion of evaluation is valid, the high variability of patients and therapists suggest that a more insightful approach to modeling and evaluation may be valuable to determining the ubiquity of a modeling method. Specifically, formulating the criteria can be done in such a way that the modeling and evaluation method is grounded in occupational therapy principles. This can be done by abstracting the criteria for evaluation from explicitly replicating an action to emulating strategies that determine that action. Evaluating modeling methods in such a way would more adequately address performance when considering the full scope of a clinical setting.

C. Organization

To fulfill the requirements of this paper, this document is organized as follows. First, a literature review on rehabilitation strategies used by therapists and methods for modeling therapist assistance will be given. Then, the objectives, significance and scope of this research will be described and followed by a description of the exoskeletal and data collection systems. Next, the theoretical framework for the machine learning algorithms and evaluation methods will be presented. After this, the methodology for data collection, processing and analysis will be described. Finally, the results of this research will be reported and discussed.

2. LITERATURE REVIEW

A. Therapist Strategies

As previously stated, a critical contributor to patient motor learning outcomes is active patient engagement in the exercises. In a review of methods for incorporating neurophysiological perspectives into robotic devices [10], several therapist strategies were outlined to promote active physical and cognitive engagement from the patient. Adapting the assistance provided by the therapist can prevent overreliance on therapist support which would otherwise allow for a patient to reduce physical effort and automate their actions. A therapist can also adjust the difficulty or cognitive challenge of a task by providing additional impedance or altering the task environment. Additionally, providing therapist feedback can help motivate the patient and facilitate the desired motions for the proprioceptive input needed to activate neuroplastic mechanisms.

Another widely accepted rehabilitation strategy is functional task performance. Rehabilitation training within the context of the desired functional task (e.g. walking) is an approach often employed to improve patient outcomes. In [11], the reviewed studies relating to context specific training repeatedly show that this strategy more significantly impacts task performance over nonfunctional exercises like strength training. The suspected mechanisms that are actuated during performance of functional task and their effects on neural and cognitive systems is explained in [4]. Improved outcomes from performing a functional task are currently believed to be caused by the sensory inputs associated with the interaction between the patient and their environment and the integration of task-specific sensory inputs that are experienced during task performance. In other words, additional sensory inputs are available besides the peripheral sensory

inputs generated in response to the proprioceptive stimuli. Consequently, the mechanisms of neural plasticity can be actuated to a greater degree. An additional benefit of this strategy is provided in [12] where task-specific exercises can assist in not only the natural recovery of motor function but provide patients with a means to develop locomotion strategies that compensate for the impaired movement which some will never fully recover.

The actions, strategies, and mechanisms involved in achieving positive rehabilitation outcomes are complex and often have many competing theories for how they should be defined. However, the methods and definitions defined in the reviewed literature were used to develop a basic model for how therapist strategies associate with different levels of the rehabilitation process. This model will later be used to develop the criteria for evaluation of therapist strategies and is shown in Figure 1.

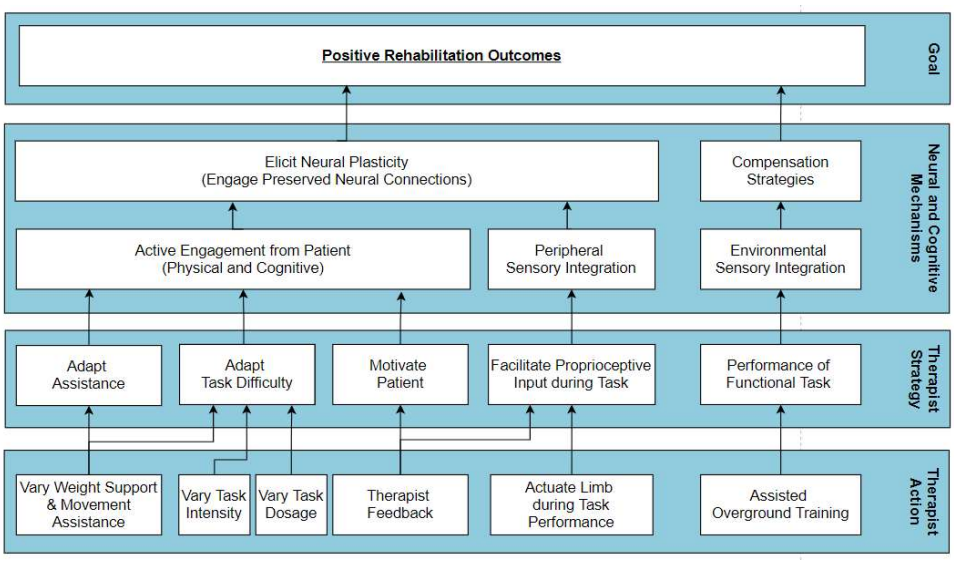

Figure 1: Summary of Relevant Therapist Strategies

B. Modeling Therapist Assistance

The first problem that is presented when modeling therapist-patient interactions is that a valid method for capturing the patient kinematics and therapist assistance must be created. Most methods for capturing patient kinematics include using either inertial measurement units (IMU) [13], a motion capture system [14], or kinematic linkages attached to the patient [15-16]. Methods for capturing therapist assistance typically involves force or pressure sensors located at critical points along the human body [13-16].

In [13], IMUs and force sensors were placed at the hip to capture accelerations of the center of mass of the patient and the therapist's assistive force to facilitate lateral balance. Using this data, a model for capturing timing and magnitude of lateral balance assistance was developed. A critical assumption in this work is that the patients center of mass is a good predictor of therapist assistance forces. This assumption seemed to be

validated by the fact that the algorithm was able to accurately predict the therapist assistance 87% of the time. Additional analysis was performed on three features: magnitude, duration, impulse, and the plane in which the assistance took place. All of these metric does begin to incorporate metrics relating to the field of rehabilitation but do not necessarily measure high-level principles of OT like therapist strategies.

In [15], patient kinematics were captured by attaching a zero-impedance kinematic arm to the patient and measuring the displacement of the links. Therapist assistance was measured by having the therapist actuate force torque sensors attached to the links. The goal of this study was to identify how therapist variation affects assistive characteristics. Specifically, therapist variability considered the different skill level of trainers. This feature was shown to have a strong correlation with better knee extension and fewer episodes of toe dragging. Each dependent variable was measured by a having a rehabilitation expert watch footage of the experiments and rate the performance of the trainers in various assistance characteristics. The method for evaluation in this study exemplifies the principles of grounded evaluation. Primarily this is because evaluation addressed performance of the trainers in terms that relate to and can be understood by an expert of neurophysiology (e.g. proper knee extension). This is in contrast to the dissociated, but still valid, methods for statistical evaluation of the predicted assistance (as seen in the first three metrics in [13]).

3. RESEARCH OBJECTIVES

A. Objectives

This research aims to provide a deeper insight on the relative advantages of various machine learning algorithms within the context of modeling therapist-patient interaction for gait rehabilitation. To accomplish this, a framework for evaluating machine learning algorithms that is grounded in the principles of occupational therapy must be developed. Therefore, the first objective is to identify:

1. What therapist strategies can be quantitatively evaluated given the limitations of the system.
2. Methods for grounding evaluation in principles of occupational therapy.

The second objective is to evaluate and gain insight on different modeling approaches. Mainly, this objective is concerned with using the grounded evaluation criteria to identify:

1. How well the algorithms emulate therapist strategies and their practicality in a clinical setting.
2. Possible sources for success or failure of each algorithm to emulate therapist strategies.

Answering these questions will be done by comparatively evaluating the capabilities of ordinary least squares regression (OLS), gaussian process regression (GPR), and inverse reinforcement learning (IRL) algorithms to accurately emulate therapist strategies within the context of a one degree of freedom knee-exoskeleton.

B. Significance and Potential Contributions

The intended contributions of this research primarily relate to the field of rehabilitation robotics. Specifically, this research aims to suggest a more insightful approach to modeling therapist assistance than some current methods that disproportionately consider, or exclude all together, a neurophysiological perspective. This insight creates the potential to broaden the scope of evaluation to include principles found in clinical settings. Significant conclusions from this work have implications on moving modeling approaches that would otherwise demonstrate this issue to a more well-rounded and complete perspective. Furthermore, this may provide an opportunity for devices to be more widely accepted by therapists and more effectively penetrate into practical settings.

C. Scope and Limitations

This research is framed within the context of a wearable 1 degree of freedom knee exosuit (Figure 3). The purpose of this device is not to replace or fully replicate the function of a therapist but rather to supplement a subset of therapist tasks. With this in mind, the exosuit was designed to provide assistance using a single actuator attached to the knee. This implies that the moment of actuation around the knee, also interpreted as device-assistance, is normal to the sagittal plane and that assistive forces that fall outside of this definition are intended to remain in therapist control. Consequently, features like lateral assistance (e.g. facilitation of symmetric weight bearing and balance) cannot be properly defined within the sagittal plane and are therefore not considered to be observable. It follows that the scope of therapist strategies capable of being used as

methods for evaluation is also limited. A detailed procedure for identifying which strategies are applicable is available in Section 5.D.

Relating to the second objective of this research, a breadth-first approach was chosen to select the algorithms that will be evaluated using the proposed methods. Three algorithms with high relative novelty were chosen to be the subjects of this research. Even though there are many more standardized modeling methods that are available in the literature, this small sample provides enough comparisons to develop an initial insight on the modeling approaches and evaluation criteria.

A significant limitation that was experienced during this study was that access to patients for data collection was severely limited. The initial intent was to evaluate data from multiple patients but due to technical issues in the data collection system and the limited access to patients, valid data from one patient was able to be collected. Therefore, this research is framed in the context of a case study.

4. DEVICE DESCRIPTIONS

A. Data Collection System

A wireless data collection system was developed to collect the training and testing data uses several wearable sensors that aim to capture the patient kinematics, ground reaction forces and assistive torque around the knee that is provided by the therapist. As this research mainly focuses on the modeling methods used for analyzing this data, further description of sensors like these can be found in [17].

Nonetheless, two IMUs are placed on the patient's leg to measure thigh and shank displacements. Additionally, a smart shoe was worn that contains four pressure sensors

to capture the current gait phase of the patient. An array of similar pressure sensors is then placed on both sides of the knee that will measure the location and magnitude of the force applied by the therapist on the patient. This system provides a relatively high resolution of observable features for an independent and mobile platform. A picture of the data collection system is given in Figure 2.

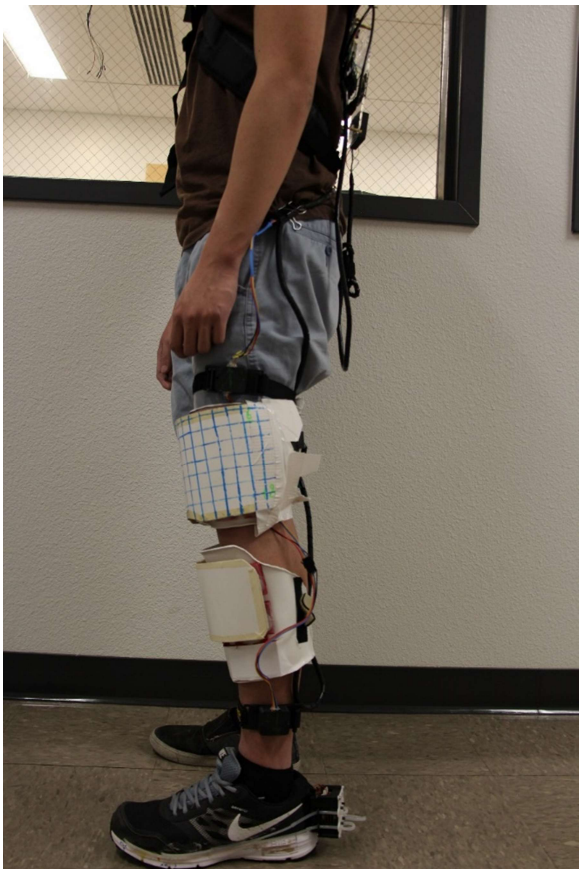

Figure 2: Data Collection System

B. Exoskeletal System

As previously stated, the considered modeling algorithms are being developed in the context of a one degree of freedom knee exosuit. This device uses a compliant

actuator that applies a torque located around the knee. The axis of rotation for this assistive torque is normal to the sagittal plane. Two links attached to the actuator are then connected to the patient's thigh and shank using several hook-and-loop fasteners. The sensors in the data collection system were also implemented into the exoskeleton system to as a way of implementing these algorithms in the future. Other peripheral devices like controllers and batteries are attached to the hip using a padded waist strap. Figure 3 provides an image of the exoskeletal system in use.

Figure 3: Knee Exoskeleton Attached to Leg

5. THEORETICAL FRAMEWORKS

The first three topics covered in this section have to do with the theoretical frameworks involved in modeling therapist assistance. This process can be framed as a

problem of learning from demonstration. The goal of learning from demonstration is to use a set of demonstrated trajectories to recover a map, also known as a policy, that relates a set of observable states to actions. Typically, these demonstrations are gathered by observing a human expert performing the task. Approaches to solving the learning from demonstration problem can be divided into two major categories: behavioral cloning and apprenticeship learning.

Behavioral cloning methods attempt to directly mimic the observed expert trajectories. In other words, behavioral cloning uses supervised learning algorithms to directly learn a policy [18]. However, this method of learning has limitations in that the efficacy of the model can quickly become poor when it is applied to states that were not observed in the initial training data. This is of particular interest when attempting to learn in large or complex systems since capturing the full set of expert trajectories is likely infeasible [19].

This problem is the motivation for using apprenticeship learning algorithms. Apprenticeship learning attempts to learn the expert's reward function, instead of a policy, that expresses an agent's perceived utility of visiting a state. This reward function can also be interpreted as the goals of the agent. The action of the agent is then determined by selecting the one that will move the agent to the state with the highest reward value. This approach implies that observing the full set of trajectories is not required as long as the goals of the expert remain unchanged throughout all possible trajectories. Given this condition, apprenticeship learning "is the most succinct, robust, and transferable definition of the task" when learning from demonstrations [19].

Two algorithms for behavioral cloning and an algorithm for apprenticeship learning through inverse reinforcement learning were selected as the methods for modeling therapist assistance. Specifically, the chosen algorithms include ordinary least squares regression (OLS) [20], gaussian process regression (GPR) [21], maximum entropy (MaxEnt) inverse reinforcement learning (IRL) [22]. The justification for these algorithms is that each has a high relative novelty that increases the breadth of insights that can be gained.

The last topic covered in this section relates to developing a framework for grounded evaluation of the proposed algorithms.

A. Ordinary Least Squares Linear Regression

OLS is one of the most commonly used regression methods and is often the first learning algorithm that people are exposed to. This is because OLS is fairly intuitive, and the process can easily be visualized through the use of images like Figure 4. Following the formulation for linear regression given in Section 9.2 of [20], OLS aims to solve for a class of linear regression predictors by minimizing the squared loss defined by the deviations between the observed and predicted outputs. These deviations can be seen in Figure 4 by the vertical lines between the observed data points and the fitted polynomial.

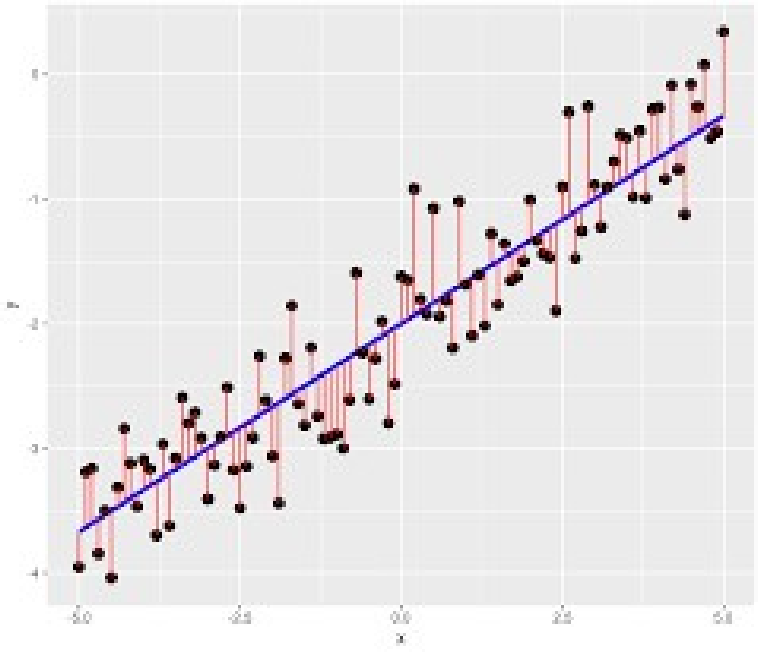

Figure 4: Error of One Degree Polynomial [23]

A one-dimensional polynomial of degree n that describes the regression curve, given the class of predictors **x** and coefficients **a**, can be expressed in the form of

$$p(x) = a_0 + a_1 x + a_2 x^2 + \cdots + a_n x^2 \tag{1}$$

Given a training data set $\boldsymbol{S} = (\boldsymbol{X}, \boldsymbol{Y})$, we can define the empirical risk minimization problem as our objective function that describes the squared loss:

$$arg\min_{\boldsymbol{w}} L_s(h_w) = \operatorname{argmin}_{\boldsymbol{w}} \frac{1}{m} \sum_{i=1}^{m} (< \boldsymbol{w_i}, \boldsymbol{x_i} > y_i)^2 \tag{2}$$

This problem can then be framed as an optimization problem by calculating the gradient of this objective function and rewriting it in the form of $\boldsymbol{Aw} = \boldsymbol{b}$:

$$\frac{2}{m}\sum_{1=1}^{m}(< \boldsymbol{w}, \boldsymbol{x_i} > y_i)\boldsymbol{x_i} = 0 \tag{3}$$

$$\mathbf{A} = \left(\sum_{1=1}^{m} \boldsymbol{x_i}\boldsymbol{x_i^T}\right), \boldsymbol{b} = \left(\sum_{1=1}^{m} \boldsymbol{y_i}\boldsymbol{x}_i\right) \tag{4}$$

These results can be extended to polynomial predictors by reducing this problem to the previously formulated OLS method. By defining a map $\psi: R \to R^{(n+1)}$such that $\psi(x) = (1, x, x^2 \ldots x^n)$ we can write our polynomial expression in the form of

$$p\big(\psi(\mathrm{x})\big) = a_0 + a_1 x + a_2 x^2 + \cdots + a_n x^2 =< \boldsymbol{a}, \psi(x) > \tag{5}$$

and find the optimal vector of coefficients using the method described above.

OLS requires a few assumptions. First, it assumes that there is a linear relationship between the independent and dependent variables and that the dependent variable is continuous. It also assumes that errors are normally distributed, have homoscedasticity, are correlated with neither the independent nor dependent observations and are not caused by measurement errors [24]. Additionally, OLS is susceptible to strong influence from outliers and cause unwanted influences in the final model [25]. While not all of these conditions can be met by the observed dataset for therapist assistance, a basic model can be formulated to serve as a comparison for the other learning methods.

B. Gaussian Process Regression

GPR is a machine learning tool that is able to produce powerful results by learning the probability distribution over all functions that fit the training data. A

significant advantage of GPR is that the variance of this distribution can be exploited as a means to interpret confidence of the prediction μ_i. In the context of developing models for a wearable exosuit, this is a significant result that can be used as a linear gain variable or used to determine if the system should assist at all [21].

It is important to note that this hypothesis class contains infinitely many functions that, for a given set of training points **X**, can perfectly fit the data. To that end, a core goal of GPR is to model the underlying distribution of observed predictors $\boldsymbol{X}$ together with the set of observed outputs $\boldsymbol{Y}$ as a joint probability distribution $P_{\boldsymbol{X},\boldsymbol{Y}}$ that describes the possible prediction values contained in the distribution of functions

GPR relies on Bayesian Inference as a means to update the current hypothesis as new information is introduced to the system. This allows for the analysis of the conditional probability $P_{X|Y}$ which is also distributed normally since the initial gaussian distribution is closed under conditioning [1].

However, this hypothesis class is infinitely large and is not very powerful. Therefore, GPR restricts this class by assigning a probability to each function and creating a probability distribution over the functions. This distribution has a mean function $\boldsymbol{\mu}$ and covariance matrix $\boldsymbol{\Sigma}$ that describes which type of functions from the space of all possible functions are more probable. Entries in the covariance matrix $\boldsymbol{\Sigma}$ are determined by a kernel *k* which will be discussed in Section 5.B.i.

The restricted class of functions and their probabilities can then be used to extract, given a set of predictors $\boldsymbol{x_i}$, the mean prediction μ_i value and the variance ${\sigma^2}_i$ associated with that possible prediction.

Following the formulation given in [26], The first step is to define an initial, or prior, distribution P_X where no training data has been introduced and the assumed mean is zero. This assumption is necessary for the later conditioning of the distribution. Figure 5 provides an example of a prior distribution that has not observed any training points and therefore has a mean μ =0 described by the dark purple line. The region lightly shaded purple describes the interval in which the algorithm is 95% confident that the true prediction lies within.

Figure 5: Prior Distribution before Observing Training Points [27]

P_x can be updated by first determining the marginalized probability distribution of the joint distribution $P_{X,Y}$

$$P_{X,Y} = \begin{bmatrix} X \\ Y \end{bmatrix} \sim \mathcal{N}(\mu, \Sigma) = \mathcal{N}\left(\begin{bmatrix} \mu_X \\ \mu_Y \end{bmatrix} \begin{bmatrix} \Sigma_{XX} & \Sigma_{XY} \\ \Sigma_{YX} & \Sigma_{YY} \end{bmatrix}\right) \tag{6}$$

$$p_X(x) = \int p_{X,Y}(x, y)dy = \int p_{X|Y}(x|y)p_Y(y)dy \tag{7}$$

Using conditioning, the predictive distribution $P_{X|Y}$ can be found from the joint distribution $P_{X,Y}$. This conditional distribution $P_{X|Y}$ constrains the set of possible functions to pass through the training points (±ε). Figure 6 and Figure 7 describe progressively more constrained posterior distribution as more observations are introduced through the process of Bayesian Inference.

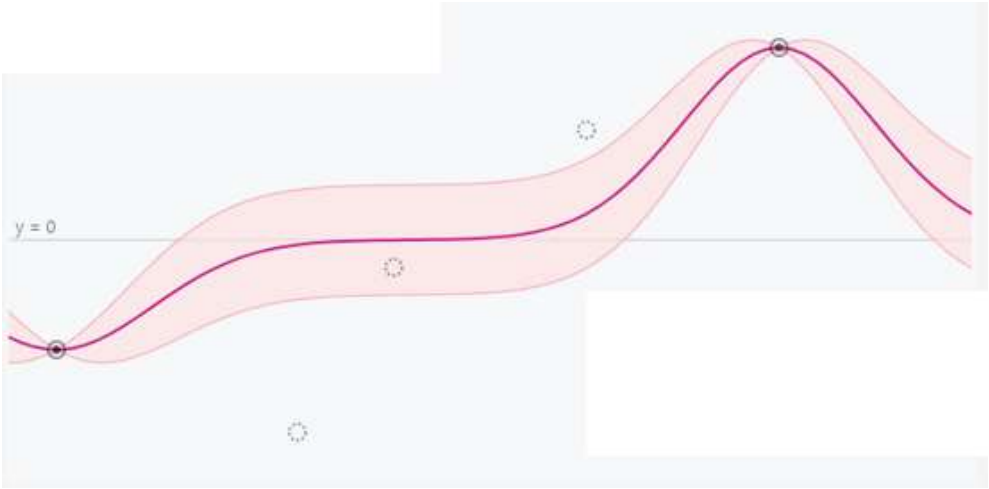

Figure 6: Posterior Distribution after Observing Training Two Points [27]

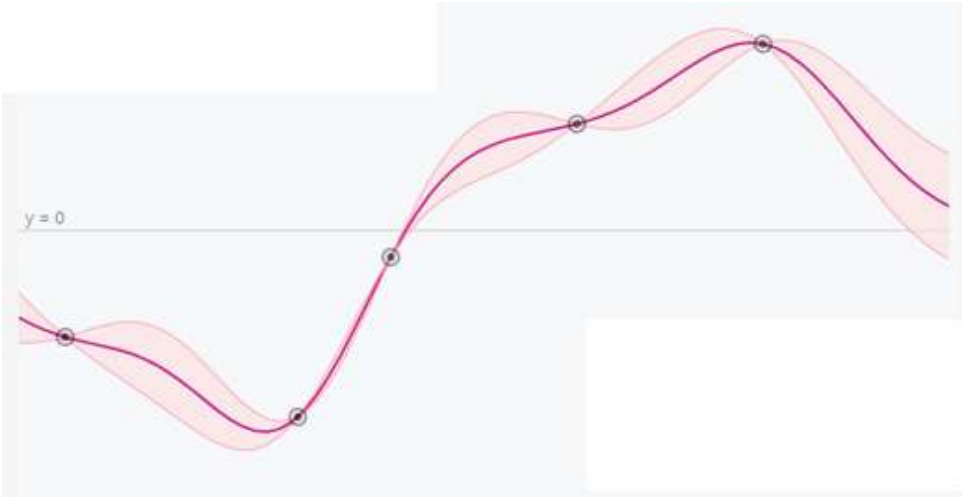

Figure 7: Posterior Distribution after Observing All Training Points [27]

By using marginalization of each random variable, the mean $\boldsymbol{\mu_i'}$ and standard deviation $\boldsymbol{\sigma_i'} = \boldsymbol{\Sigma_{ii}'}$ for i^{th} observed output Y_i. These variables can then be used to provide most probable output and an interpretation of confidence that $\boldsymbol{\mu_i'}$ is the output of the underlying function.

i. Kernels

Another powerful feature of GPR is the ability to include prior knowledge into the system by defining a covariance function *k* that is also referred to as a kernel. This kernel describes the shape of the distribution and the characteristics of the predicted function. This is possible since the covariance matrix is determined by evaluating the covariance function pairwise to all points. Kernels provide a map from two points $t, t' \in \mathcal{R}^n$ to a similarity measure between the two:

$$k: \mathcal{R}^n x \mathcal{R}^n \rightarrow \mathcal{R}, \Sigma = Cov(X, X') = k(t, t') \tag{8}$$

Kernels have many standardized forms and can be combined in various ways to achieve the desired effect. A useful guide for determining a effective kernel is to use a kernel cookbook [28]. Figure 8 provides a basic example of the commonly used linear and periodic kernels and the effects of varying combinations on the posterior distribution.

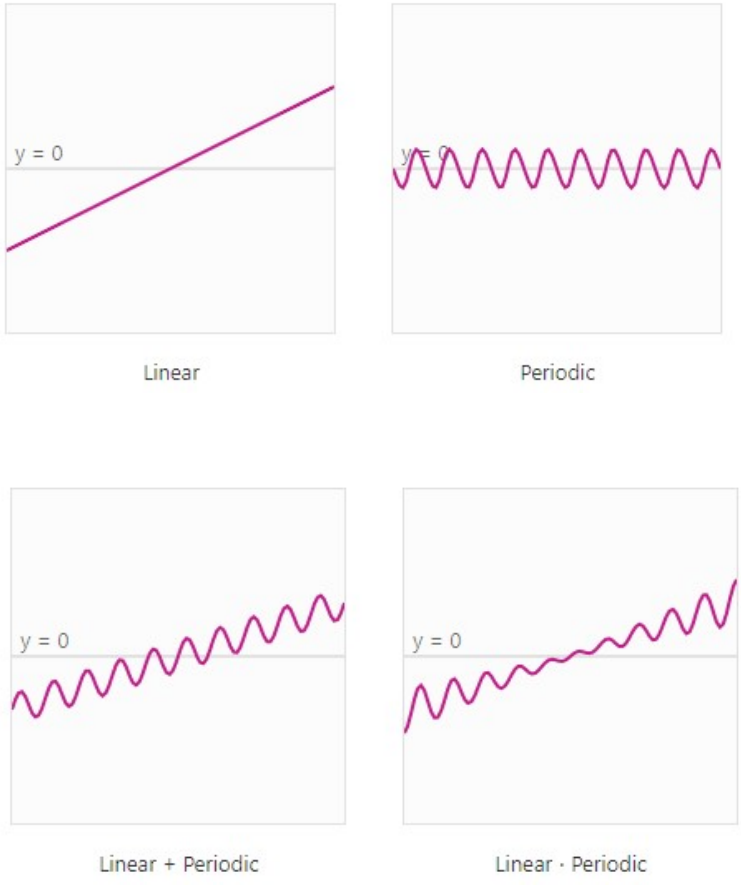

Figure 8: Effects of Kernel and Kernel Combinations on Posterior Distribution [27]

C. Maximum Entropy Inverse Reinforcement Learning

To address the IRL problem, we must first structure the space of learned policies to be a Markov Decision Process (MDP) where agents optimize an unknown reward

function by assigning reward weights that make the demonstrated behavior optimal. Paths in MDPs are determined by the action choices of agent in addition to random outcomes thereby making it an appropriate framework for modeling human decision making. MDPs can be parameterized by $M = \{\boldsymbol{S}, \boldsymbol{A}, , T, \gamma, D, R\}$ where the agent's behavior is modeled with states $s \in S$, actions $a \in A$, an initial state distribution $D(s)$, transition dynamics $T = p(s'|s, a)$, reward function R(s), and discount factor $\gamma \in [0,1]$.

Also, we must assume that the agent is attempting to optimize some "true" reward function, $R^*(s) = \theta^* \cdot \phi(s_t)$ that can be expressed through a linear combination of features $\phi(s)$ and that are weighted by the true reward weights θ^*. Using this, we can determine the value of a policy $\pi(a|s)$ that maps states to a probability distribution of actions[29]. $s_t \infty$

$$V(\pi) = \theta \cdot E\left[\sum_{\mathrm{t}=0}^{\infty} \gamma^{\mathrm{t}}\, \phi(s_t)\, |\pi\right] \tag{9}$$

Where the feature expectations can be defined as the expected value of the discounted features for a given policy:

$$\mu(\pi) = E\left[\sum_{t=0}^{\infty} \gamma^{t}\, \phi(s_t)\, |\pi\right] \tag{10}$$

The algorithm proposed by Abbeel & Ng [29] the proposes finding the a policy that attempts to match the feature expectations from the expert demonstrations to a policy optimized through an iterative algorithm:

$$\left|\mathrm{E}\left[\sum_{t=0}^{\infty} \gamma^{t}\, \phi(s_t)\, |\pi\right] - E\left[\sum_{t=0}^{\infty} \gamma^{t}\, \phi(s_t)\, |\tilde{\pi}\right]\right| = |\theta^T \mu(\pi) - \theta^T \mu(\pi)| \tag{11}$$

In this framework, the "problem of imitation learning can be reduced to recovering the reward function that induces the demonstration trajectories." However, recovering the reward weights is considered an ill-posed problem since multiple weights and degenerate solutions can make the demonstrated trajectories optimal [22].

i. Maximum Entropy

Following the paper by Ziebart's et.al [22], the principle of Maximum Entropy (MaxEnt) can be used to help resolve this ambiguity. A trajectory's reward value can be described by the reward weight applied to the path's feature counts.

$$reward(\boldsymbol{f}_\zeta) = \theta^T \boldsymbol{f}_\zeta = \sum_{s_j \in \zeta} \theta^T \boldsymbol{f}_{s_j} \tag{12}$$

The MaxEnt IRL framework considers the class of all feasible paths through the MDP. It then "resolves ambiguity by choosing the distribution that does not exhibit additional preferences beyond matching feature expectations" where the distribution is parameterized by reward weights θ. Considering the space of action outcomes, *T,* and an outcome sample, o, that specifies the next state for every action. Also, under the assumption that the transition randomness has minimal effect on the behavior and the partition function, $Z(\theta)$, is constant for all $o \in T$ we can obtain an approximation of the distribution over all paths. To this end, the MaxEnt IRL algorithm suggests that we can optimize for our reward weights by maximizing the likelihood of the observations under this distribution.

$$\theta^* = \underset{\theta}{\operatorname{argmax}}\, L(\theta) = \underset{\theta}{\operatorname{argmax}} \sum_{examples} logP(\tilde{\zeta}, \theta, \mathrm{T}) \tag{13}$$

Optimization can be performed through a gradient descent algorithm where the gradient is the difference between the expected empirical feature counts and the learner's expected feature counts. This algorithm can be expressed using the expected state visitation frequency D_{s_i} by using algorithm 1 in [22].

$$\nabla L(\theta) = \tilde{\boldsymbol{f}} - \sum_{\zeta} P(\zeta \,|\theta, \mathrm{T})\mathbf{f}_{\zeta} = \tilde{\boldsymbol{f}} - \sum_{\zeta} D_{s_i}\boldsymbol{f}_{s_i} \tag{14}$$

Once the reward weights are returned, the policy can be recovered through reinforcement learning methods [29]. This policy will then be used to make predictions for the model.

ii. Handling Unknown System Dynamics

The transition dynamics for a given system are often not explicitly known in the real world. This problem can be resolved by a straightforward method for estimating transition probabilities by observing the transition counts. However, it should be noted that is likely that not all possible transitions are observed and therefore the initial count for each transition should be started at one. This will prevent a unobserved transitions from having no probability of occurring [30]. Here, we treat the observed dataset as samples from the true system dynamics and normalize the observed transition counts for each state action pair to obtain an estimated state transition probability distribution.

D. Grounded Evaluation

Grounding the methods for evaluation in the principles of OT simply means that the measurements of performance should emerge from the principles and concepts that surround this field. Doing this has the potential to provide a more generalized measurement of performance that can be extended beyond the observed testing data.

In contrast, standard methods for evaluating fitted models attempt to measure the model's ability to directly reproduce the observed data. The two main metrics for standard evaluation are the coefficient of determination (r^2) and mean squared error (MSE). The coefficient of determination represents the proportion of variation of the output that is explained by the model. The mean squared error describes the average squared deviation between the predictions and the observed outputs. Similarly, the mean absolute error can be used to measure the same feature through handling positive and negative deviations by taking the absolute value instead of the square. All of these values give a valid measurement on the goodness of a model but are limited in scope. Similar to the differences between behavioral cloning and apprenticeship learning, the results from these standard evaluation methods can only be used to make conclusions over the observed dataset.

Figure 9 provides an illustration providing examples of how evaluation metrics can be progressively grounded in OT. Weakly grounded methods, on the bottom, are the standard evaluation metrics that measure the performance of the model but do not include any considerations for neurophysiology. The middle section of this figure details intermediately grounded methods for evaluation due to the fact that the measurements emerge from the context of rehabilitation but do not capture any specific principle or

strategy used by the therapists. These measurements are concerned with describing the deviation from the observed characteristics of assistance $\boldsymbol{C}$. A full list of variable definitions for $\boldsymbol{C}$ can be found in Table 1. Finally, the grounded evaluation methods can be found at the top of the figure. These metrics directly relate to and intend to capture the strategies to actuate the neurophysiological mechanism used in rehabilitation.

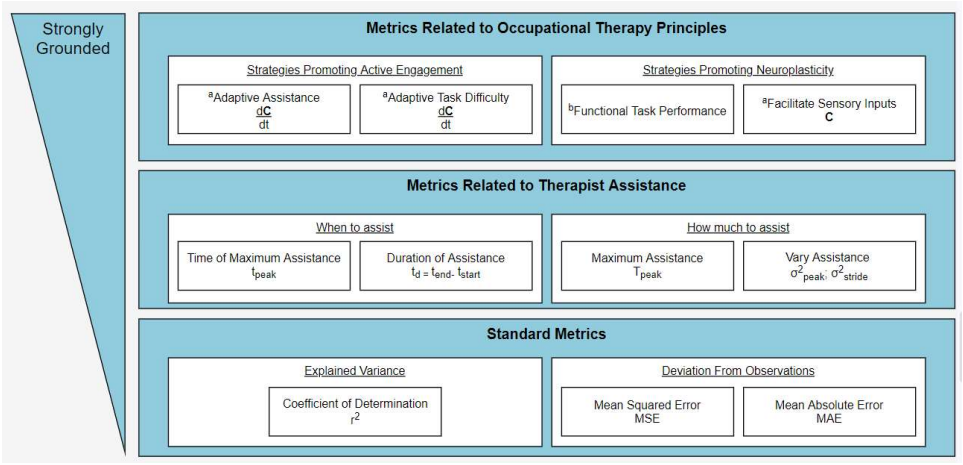

Figure 9: Standard and Grounded Evaluation Metrics [a] $\boldsymbol{C}$ refers to the characteristics of assistance described in Table 1 [b] Functional task performance does list a quantifiable measurement because this strategy is either used or not and is therefore subject to continuous evaluation.

Table 1
Characteristics of Assistance

Variable	Units	Name	Description
$\bar{\tau}_{peak}$	Nm	Mean peak torque	The mean of all of the maximum values evaluated on a per gait cycle basis.
τ_{sig}	Nm	Significant torque	Threshold that is considered significant actuation. This is considered because torque readings are received when the therapist has their hand on the sensors but are not in fact actuating. For this analysis, significant torque is considered to be any value greater that 0.5 Nm.
t_{start}	%GC	Significant actuations start	The earliest time, in percent gait cycle, that the torque first exceeds the significant torque τ_{sig} threshold.
t_{end}	%GC	Significant actuation end	The latest time, in percent gait cycle, that the torque first exceeds the significant torque τ_{sig} threshold.
$\Delta\, t_{sig}$	%GC	Significant actuation duration	The duration, in percent gait cycle, for which significant torque τ_{sig} is observed
$\bar{t}_{peak}$	%GC	Mean peak time	Meantime, in percent gait cycle, that peak torque occurs
σ^2_{peak}	Nm^2	Peak torque variance	The variance between peak actuation torques $\boldsymbol{\tau}_{peaks}$
σ^2_{total}	Nm^2	Actuation variance	The variance of all predicted torques during any part of the gait cycle

Several of the strategies summarized in Figure 1 are simply not within the collected data's capability to measure or exosuit' s ability to perform. Therefore, this

model must be reduced to include only strategies that can be captured in a meaningful way. After excluding these features from the model, three main strategies are left for evaluation: adaptive assistance, adaptive task difficulty, and facilitation of proprioceptive inputs. Figure 10 illustrates how the previously model for the reviewed therapist strategies was modified to exclude features (grey) in order to make it fit this evaluation.

It should be noted that the exosuit can only provide assistive forces around the knee and can consequently only adapt its assistance. However, an interpretation of adapting task difficulty is still available since providing less assistive forces can be considered a method for increasing the task difficulty. This interpretation is weak since more practical task adaptation strategies include adding impedance (e.g. elastic band training). Nonetheless, these two adaptation strategies would present themselves in the exact same way when considering the amount of force actuated by the exosuit. These two adaptation strategies are therefore consolidated into a single feature for the purpose of evaluation.

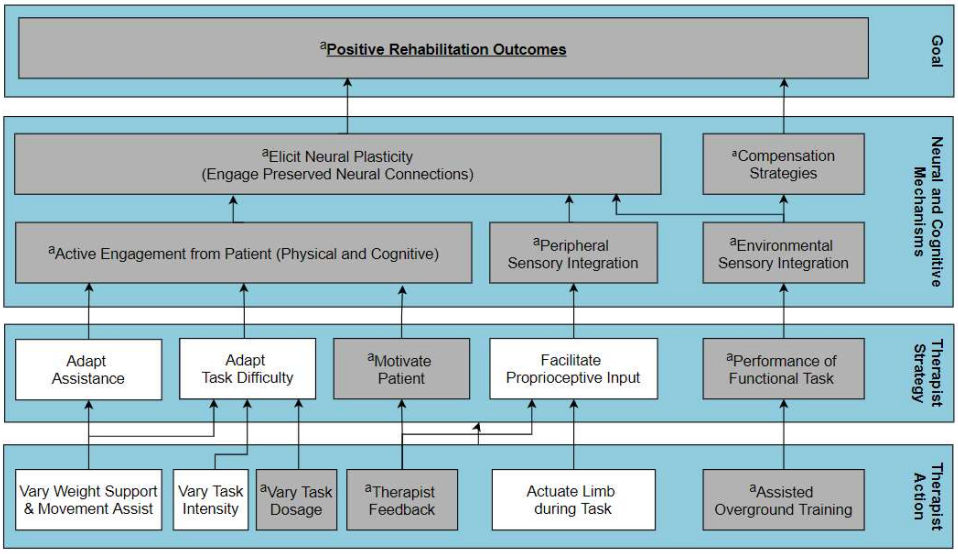

Figure 10: Modified Therapist Strategy Model [a] Indicates that a feature is not within the capabilities of the exosuit to perform, measure or effect. Consequently, these features is either not feasible or not applicable for the process of evaluation of the modeling methods.

Now that the strategies that will be evaluated have been selected, three principal questions arise as the foundation for developing subsequent tests:

1. How well do the algorithms emulate the characteristics of assistance demonstrated by the therapists?
2. How well do the algorithms emulate the adaptation of assistance?
3. To what extent can an algorithm emulate strategies demonstrated by different therapists?

To address these questions, two different methods for analysis were created. The first method is to calculate the $\boldsymbol{C}$ of each algorithm and compare to each of the observed $\boldsymbol{C}$ of therapist 1 and 2. This requires six comparisons that are grouped per therapist:

$$\boldsymbol{C}_{d1} = \left(\boldsymbol{C}_{therapist\ 1} - \boldsymbol{C}_{OLS}, \boldsymbol{C}_{therapis\ \ 1} - \boldsymbol{C}_{GPR}, \boldsymbol{C}_{therapis\ \ 1} - \boldsymbol{C}_{IRL}\right)$$

$$\boldsymbol{C}_{d2} = \left(\boldsymbol{C}_{therapist\ 2} - \boldsymbol{C}_{OLS}, \boldsymbol{C}_{therapist\ 2} - \boldsymbol{C}_{GPR}, \boldsymbol{C}_{therapist\ 2} - \boldsymbol{C}_{IRL}\right)$$

The second method for analysis focuses on the adaptation for CoA over the course of each therapists' session. This can be done by observing the trend of CoA over time. Since the collected data does not observe time as one of the features, strides t_s will be used for the time domain. Comparisons for each algorithm can be expressed as follows

$$\frac{\partial}{\partial \mathrm{t_s}} \boldsymbol{C}_{d1} = \frac{\partial}{\partial \mathrm{t_s}} \left(\boldsymbol{C}_{therapist\ 1} - \boldsymbol{C}_{OLS}, \boldsymbol{C}_{therapist\ 1} - \boldsymbol{C}_{GPR}, \boldsymbol{C}_{therapist\ 1} - \boldsymbol{C}_{IRL}\right)$$

$$\frac{\partial}{\partial \mathrm{t_s}} \boldsymbol{C}_{d2} = \frac{\partial}{\partial \mathrm{t_s}} \left(\boldsymbol{C}_{therapist\ 2} - \boldsymbol{C}_{OLS}, \boldsymbol{C}_{therapist\ 2} - \boldsymbol{C}_{GPR}, \boldsymbol{C}_{therapist\ 2} - \boldsymbol{C}_{IRL}\right)$$

Analysis can then be performed between the different therapists. This will allow insights on if the algorithm is able to extend its presentation of strategies across multiple therapists that may be providing different strategies.

$$\frac{\partial}{\partial \mathrm{t_s}} \boldsymbol{C}_{d1} \text{ x } \frac{\partial}{\partial \mathrm{t_s}} \boldsymbol{C}_{d2}$$

Table 2 presents a summary of the above formulation and how it relates to each respective therapist strategies and Figure 11 provides a high-level model for how these methods were formulated.

Table 2
Summary of Methods for Grounded Evaluation

Therapist Strategy	Question	[a]Analysis
Facilitate appropriate proprioceptive input	How well can an algorithm emulate the CoA demonstrated by the therapists?	$\boldsymbol{C}_{d1}$ and $\boldsymbol{C}_{d2}$
Adaptive assistance and task difficulty	How well can an algorithm emulate adaptation strategies?	$\frac{\partial}{\partial t}\ \boldsymbol{C}_{d1}$ and $\frac{\partial}{\partial t}\ \boldsymbol{C}_{d2}$
Adaptive assistance and task difficulty	To what extent can an algorithm emulate strategies that are different ?	$(\frac{\partial}{\partial t}\ \boldsymbol{C}_{d1})$ x $(\frac{\partial}{\partial t}\ \boldsymbol{C}_{d2})$

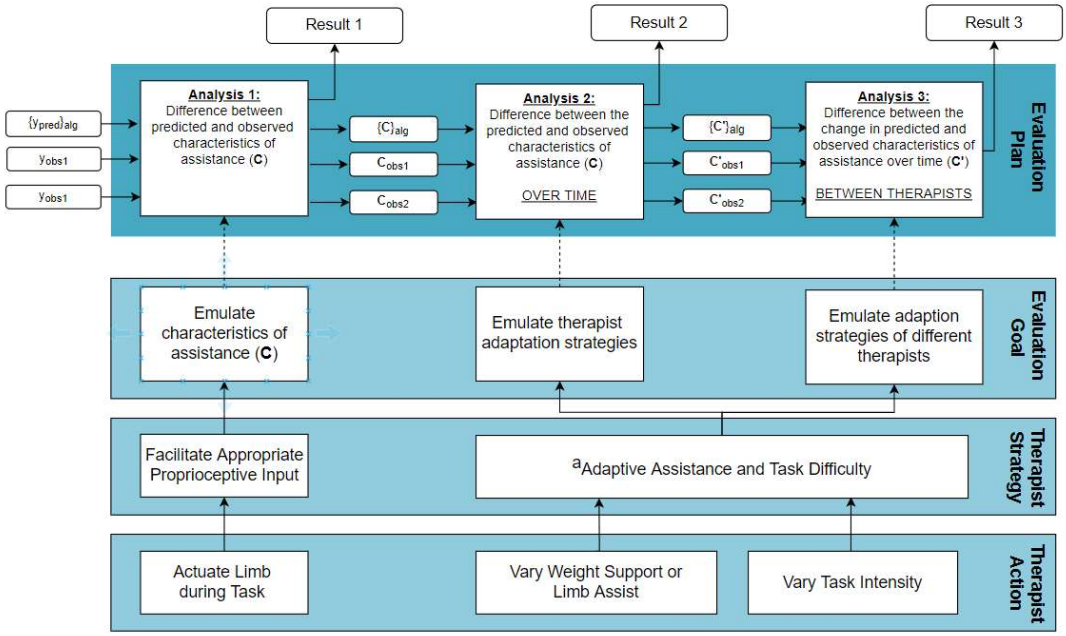

Figure 11: Grounded Evaluation Plan

[a] Strategies for adaptive assistance and adaptive task difficulty were combined into a single feature since they are presented in the same way in the exosuit.

6. METHODOLOGY

A. Sources of Data

Data was collected from 4 patients during an in-person visit to a Barrow Medical Institute Treatment Center. The targeted group of patients are individuals presented with hemi-paretic gait with knee instability on the affected side during stance phase, who can ambulate with contact guard assist or less, with Manual Muscle Testing (MMT) of knee flexion/extension equal to or greater than 2/5.

Three independent sessions lasting approximately five minutes were conducted during a single visit to the clinic. Each session consisted of the patient walking with different levels or sources of assistance. In the first session, the patient received minimal to no assistance except for balance and weigh support when needed. In the next session data was collected while one therapist provided movement assistance and the other provided weight support when needed. The last session the therapists switched roles. A member of the exosuit research team was present during each of these sessions to ensure that the data collection system maintained a proper fit to the patient and was operating appropriately. After data collection, all identifiers were removed from the data and stored on a password protected server.

Patients were screened by the therapist to ensure they meet the following criteria to be an eligible candidate for this study:

1. Male or female, between the ages of 18-60 years
2. Weigh between 110-200 lb. (to be able to fit in the data collection system)
3. Skin intact where it will interface with the sensors and markers

4. At least 100° of knee flexion to bilateral lower extremities via passive range of motion
5. Manual Muscle Testing (MMT) of knee flexion/extension equal to or greater than 2/5
6. Modified Ashworth of hemi-paretic lower extremity less than or equal to 1+
7. Ambulate with contact guard assist or less for up to 5 minutes with or without the use of single point cane and/or ankle foot orthosis (AFO)
8. Present with hemi-paretic gait with knee instability on the affected side during stance phase
9. Willing and able to provide written informed consent in compliance with the regulatory requirements. If a subject is unable to provide written informed consent, written informed consent may be obtained from the subjects' legal representative (LAR).

Criteria for exclusion from this study is as follows:

1. Unwilling or unable to comply with the requirements of this protocol, including the presence of any condition (physical, mental, or social) that is likely to affect the subject's ability to comply with the protocol.
2. Flexion contracture of greater than 10° of passive range of motion
3. Inability to understand or follow directions
4. Para-paretic gait (gait disorders on both sides)
5. Seizure activity within the last six months
6. Pregnancy
7. Unstable vitals

8. Osteoporosis
9. Any other reasons that, in the opinion of the investigator, the candidate is determined to be unsuitable for entry into the study.

B. Ethics and Human Participant Issues

No more than minimal risk will be introduced to a patient during this study. Risks include possible slips and or falls which is mitigated by the therapists present and providing support for the patient. Safety considerations regarding attaching the data collection system include quick release of attachment mechanism, an on-site supervisor, and emergency stop capabilities. All aspects of this study were reviewed and approved by the St. Joseph's Phoenix Institutional Review Board (IRB#: PHX-19-500-271-70-19).

C. Data Collection Procedure

Data collection was performed according to the following procedure:

1. Attach the data collection system to the patient by having them:
    a. Put on the pressure sensitive shoe.
    b. Strap the thigh and shank sensor shells to the leg (with the assistance of a present researcher)
    c. Put on the control backpack.
2. Have a present researcher validate that all straps are tightened and IMU's are properly oriented.

3. Have a present researcher confirm that all devices are recording data by observing the synchronous serial output.
4. Begin session one (no assistance)
    a. Have the patient stand straight for approximately 3 seconds with their knee set at zero displacement.
    b. Have the patient walk down to the end of the hallway.
    c. Have the patient turn 180 degrees and face the direction they will be walking in the next lap
    d. When the patient reaches the end of the lap, have the patient stand still for approximately 3 seconds while facing in the direction they were just walking.
    e. Repeat steps a-d for a duration of five minutes or until the patient is unable or unwilling to continue.
5. Have a researcher validate that the data collection system is still attached appropriately and did not shift during session one
6. Allow the patient to recover until they are comfortable to begin walking again
7. Begin session two (assisted by therapist #1)
    a. Have the patient stand straight for approximately 3 seconds with their knee set at zero displacement.

b. Have the patient walk down to the end of the hallway while the therapist provides assistive forces on the thigh and shank sensor shells.

c. During each stride have the therapist rate whether their assistance was good, bad or neutral

d. Have the patient turn 180 degrees and face the direction they will be walking in the next lap.

e. Have the patient stand still for approximately 3 seconds while facing in the direction they will be walking in

f. Repeat steps a-e for three total laps.

8. Begin session three (assisted by therapist #2)

    a. Follow the same procedure in step 6

9. Have a researcher assist in removing the data collection system.

10. Debrief the patient

D. Data Processing

i. IMU Data Processing

The IMU data was carefully considered in the procedure by having the patient stand still for an extended period of time both at the beginning of each lap. This was done for two reasons. The first reason was to establish a clear period where the patient is turning around. This prevents periods of unassisted steps from entering the dataset. The second reason was to reinitialize the IMUs for each lap in an attempt to counteract

drifting of the IMU values and increase the accuracy over the period of the session. The IMUs were initialized by recording the rotation, expressed as a quaternion, received during the time that the patient's knee was set to zero displacement q_0. The inverse of q_0 can then be applied to the current rotation q to obtain the relative rotation in relation, Δq, to the zero-knee displacement orientation.

$$\Delta q = q q_0^{-1} \tag{15}$$

The result of this process is a timeseries dataset that describes the rotation of the thigh and shank of the patient at given time index t. To calculate the desired features (hip and shank displacement), the initialized rotations for each IMU, Δq_{thigh} and Δq_{shank}, is applied to an initial unit vector $v_0 = [1,0,0]$ resulting in two vectors representing the thigh and shank, v_{thigh} and v_{shank}, in three-dimensional space. There are methods for calculating the acute angle between quaternions, but a vector-based approach was chosen for ease of validation through simulation and visualization. These vectors can then be used to calculate the hip and shank angle by computing the inverse cosine of the dot product of each and v_0.

$$\theta = cos^{-1}\left(\frac{v_0 \cdot v_{thigh}}{|v_0||v_{thigh}|}\right)$$

$$\theta_{shank} = cos^{-1}\left(\frac{v_0 \cdot v_{shank}}{|v_0||v_{shank}|}\right)$$

Figure 12 provides an illustration of the displacements that were recorded by the IMUs.

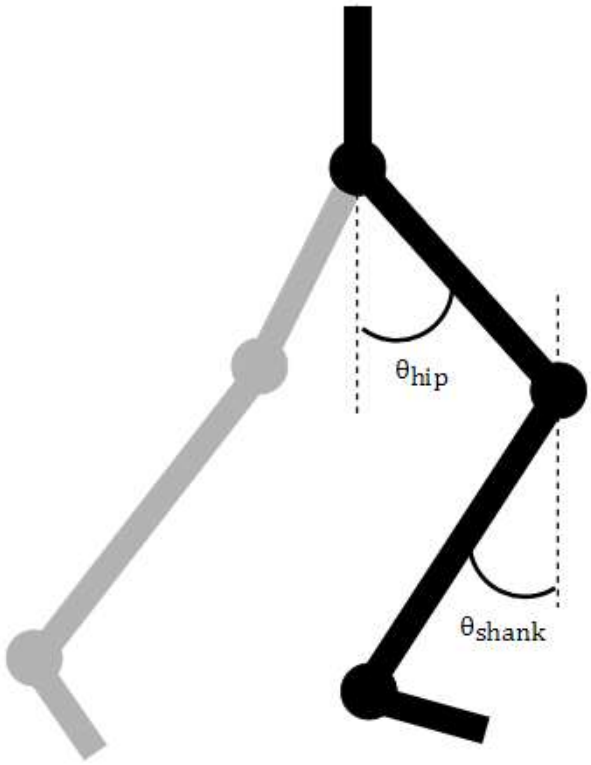

Figure 12: Calculated Hip and Shank Displacements

ii. Leg Pressure Sensors Processing

Force vectors for 18 sensors on the thigh and 10 sensors on the shank were generated. The direction of these force vectors was assigned to each sensor individually based on the location of the sensor on the curved shell. The net force for the thigh and shank were then calculated. However, since the exosuit is only a one degree of freedom devices, only forces in the sagittal plane were used to calculate the torque around the knee which is also interpreted as the therapist assistance.

iii. Shoe Pressure Sensor Processing

The shoe sensor contained four pressure sensors that measured the interaction forces between the affected leg of the patient and the ground. Using these force values, the time of heel strike and the toe leaving the ground were identified. These two values were then used to linearly interpolate the percent gait phase values in between to obtain a measurement of gait phase.

E. Generating Models

During data collection, a therapist was instructed to rate their performance of assisting the patient on a scale of good, neutral, or poor. However, some gait cycles required a therapist's full attention thereby preventing them from responding. The additional option for no response was added to the scale as a consequence. The data being considered only includes gait cycles that were rated good since other ratings introduced torques that were not readily explainable by the sensed features.

Sensed features include orientation described by quaternions of two IMUs attached to the thigh and shank, the force vector of the therapist's hand on the thigh and shank, and the location of greatest force on the foot. In order to reduce the dimensionality of the observed data, each of these sensed features were then interpreted as more simple states and actions that are directly observable by a therapist. The resulting state space was used for training all algorithms. Table 3 describes the interpretation of each sensed feature. To clarify further, the range of the gait cycle feature only considered the stance phase of the affected leg (e.i. heel-strike to push off) which is generally considered to be [0,62]% of the gait cycle. The stance phase was then rescaled to range [0,100]% and

given the variable definition s_p that express the percent progression through the stance phase. This was done because no significant and consistent actuation was observed during the swing phase and this was an opportunity to reduce the number of samples contained in the data. Figure 13 shows a full gait cycle (e.i. stance and swing phase) and the reduce range of considered observations.

To address the discrete state and action space for IRL, the joint displacements were placed in $n_\theta = 10$ uniform bins. The stance phase state was placed into $n_{s_p} = 5$ discrete bins representing the first five stages of the eight-stage model for a gait cycle described in Figure 13. These stages are initial contact (IC), loading response (LR), mid stance (MS), terminal stance (TS) and pre swing with ranges $s_p \in [0,5]$,$s_p \in (5,19]$,$s_p \in (50,81]$, and$s_p \in (81,100]$ respectively. The actions were divided into $n_a = 20$ discrete bins. The values for n_θ and n_a were manually tuned by varying these parameters and comparing the resulting models. Table 3 also provides a summary of the dimensionality reduction that was observed.

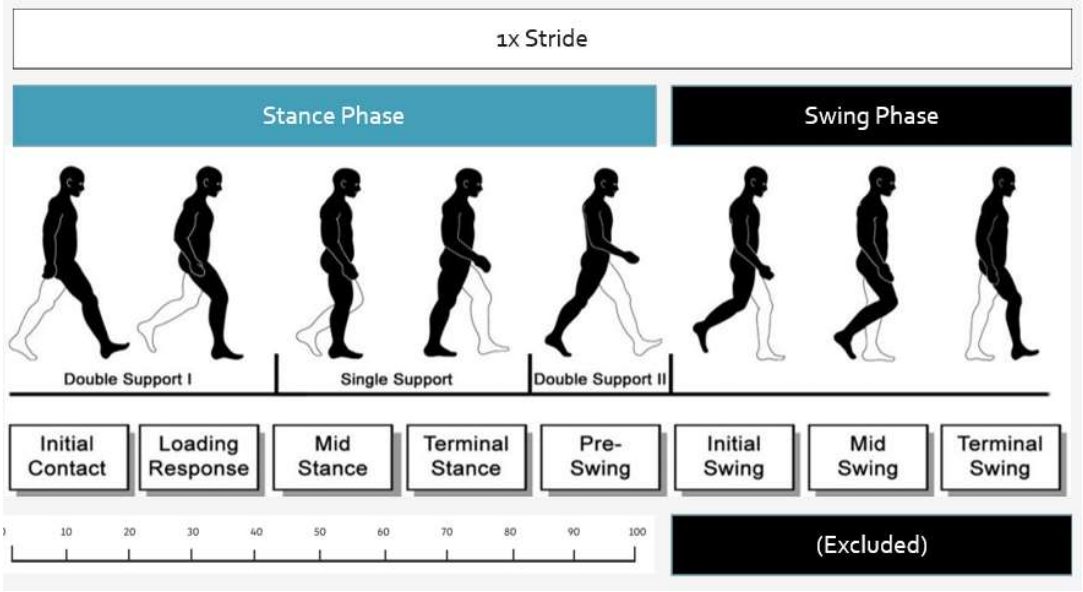

Figure 13: Reduced Gait Phase Feature to Stance Phase Feature [31]

Table 3
Summary of Dimensionality Reduction

Type	Sensed Feature	Sensed Dim.	Interpreted State	State Dim.
State	Hip IMU Quaternion	$q_{hip} \in \mathcal{R}^{1x4}$	Hip Displacement	$\theta_{hip} \in \mathcal{R}$
State	Shank IMU Quaternion	$q_{hip} \in \mathcal{R}^{1x4}$	Shank Displacement	$\theta_{hip} \in \mathcal{R}$
State	Foot Pressure Sensor	$F_{shoe} \in \mathcal{R}^{1x4}$	Percent Stance Phase	$p_s \in \mathcal{R}$
Action	Thigh & Shank Pressure Sensors	$F_a \in \mathcal{R}^{1x28}$	Torque around the Knee	$\tau_a \in \mathcal{R}$

For each proposed algorithm, the same set of predictors/states and actions were provided.

$$\boldsymbol{X} = \left[\boldsymbol{s_p}, \boldsymbol{\theta_{hip}}, \boldsymbol{\theta_{shank}}\right] \in R^{nxm}$$

$$y = \boldsymbol{\tau_a} \in R^{nx}$$

where n is the sample size and m is the number of features in each sample.

The resulting dataset contains 70 strides for therapist 1 and 32 strides for therapist 2. This data was then randomly split into 53 training strides and 17 testing strides for therapist 1 and 24. The resulting train-test split is 76%-24% respectively. Figure 14 and Figure 15 provide plots of the final training at testing datasets for each therapist over s_p.

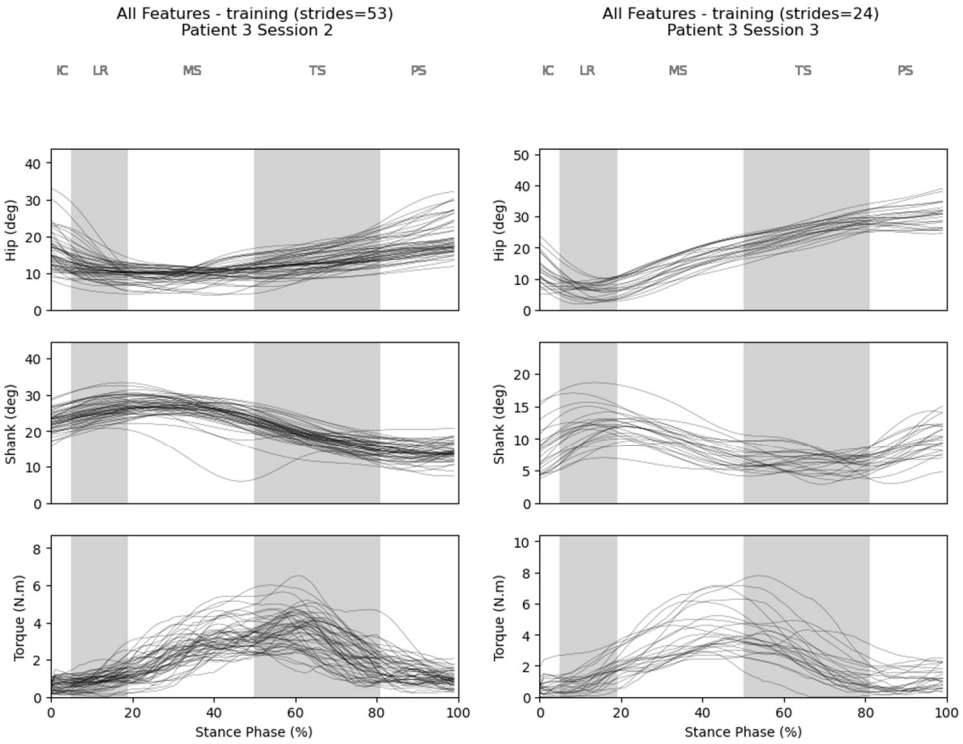

Figure 14: Training Data

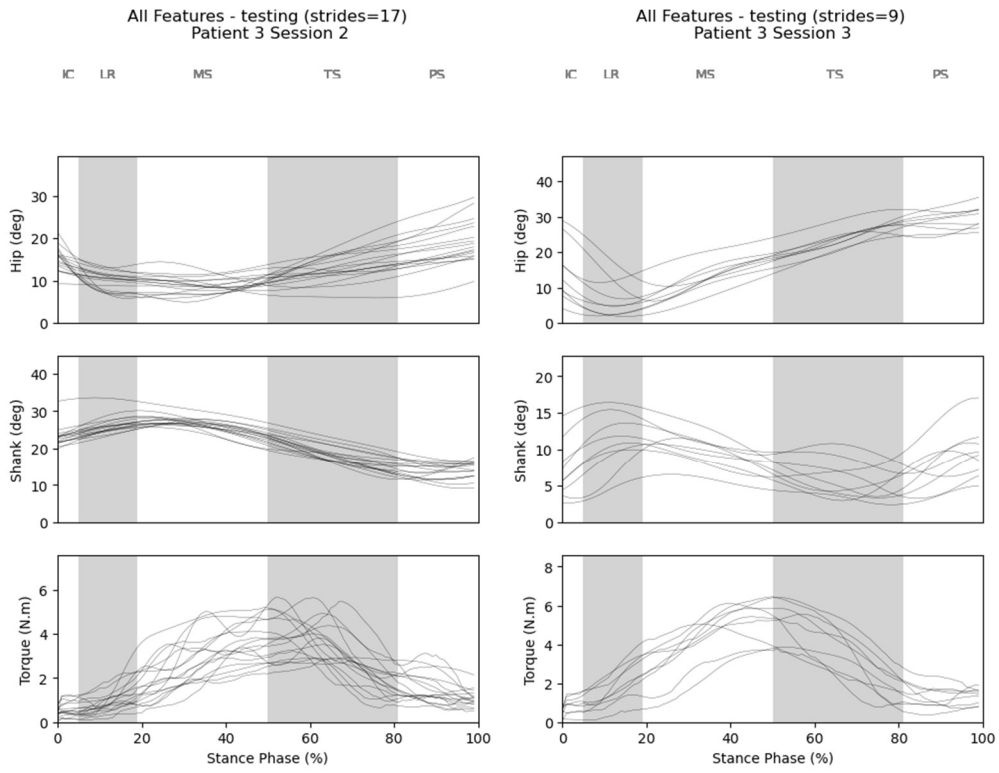

Figure 15: Testing Data

F. Data Analysis and Strategies

The objective of this research is to comparatively evaluate the capabilities of the aforementioned algorithms to accurately simulate therapist assistance and strategies within the context of a one degree of freedom exoskeleton. Using the observed states in the reserved testing data for therapist 1 ($\boldsymbol{X}_{obs1}$) and therapist 2 ($\boldsymbol{X}_{obs2}$), each algorithm will be used to generate a set of predictions for both therapist 1 and therapist 2. To simplify the notation, algorithm predictions will be grouped by the therapist training data that was used for the predictions.

$$\boldsymbol{y}_{pred}\ (\boldsymbol{X}_{obs1}) = \{y_{OLS1}, y_{GPR1}, y_{IRL1}\}$$

$$\boldsymbol{y}_{pred2}\,(\boldsymbol{X}_{obs}\,) = \{y_{OLS2}, y_{GPR}\,, y_{IRL2}\}$$

Once the algorithm predictions have been made for both therapists, three separate analyses will then be performed.

The first evaluation method will measure performance of the algorithm to directly replicate the assistance for therapist 1 (y_{obs1}) and therapist 2 (y_{obs2}). Results from $\boldsymbol{y}_{pred1}$ and $\boldsymbol{y}_{pr}$ will then be used to calculate the standard metrics for evaluation r^2 and MSE. The reported values for each prediction will be used to make comparisons on an intra-therapist and inter-therapist basis.

The second method will be used to evaluate each algorithm's ability to emulate the correct assistance to facilitate appropriate proprioceptive input. This will be done through a comparison of the characteristics of assistance $\boldsymbol{C}$ defined in Section 5.D. $\boldsymbol{C}$ will be calculated for both observed therapist outputs ($\boldsymbol{C_{obs1}}$ and $\boldsymbol{C_{obs2}}$) and for each algorithm per therapist. Notation is again simplified by grouping by therapist.

$$\boldsymbol{C_{pred1}}(\boldsymbol{y}_{pred}\,) = \{\boldsymbol{C_{OLS1}}, \boldsymbol{C_{GPR1}}, \boldsymbol{C_{IRL1}}\}$$
$$\boldsymbol{C_{pred2}}(\boldsymbol{y}_{pred}\,) = \{\boldsymbol{C_{OLS2}}, \boldsymbol{C_{GPR2}}, \boldsymbol{C_{IRL2}}\}$$

The characteristics of assistance for each algorithm with then be used to make comparisons on an intra-therapist and inter-therapist basis.

The third analysis will then evaluate the algorithms' ability to emulate therapist adaptation strategies. Adaptation strategies will be observed through how $\boldsymbol{C}$ changes for each stride t_s as the session progresses. A trendline in the form of $y = mx + b$ will be used to estimate the general behavior of how $\boldsymbol{C}$ changes. Trendlines for each characteristic in $\boldsymbol{C}$ will be generated using a one-degree linear regression algorithm. The slopes m for each trendline will then be reported and compared to their respective

therapist to evaluate how well the algorithm emulates individual therapist adaptation strategies. These results will then be used to perform an inter-therapist evaluation that will provide evidence on how well the algorithms generalize their behavior to emulate strategies of different therapists.

7. RESULTS

A. Analysis 1 Results: Standard Performance Metrics

GPR was shown to have the most desirable value for three out of four of the standard metric tests. The one metric that GPR did not exhibit the most desirable value, r^2 for therapist 2, showed approximately a 54% decrease from the calculated value for therapist 1. In contrast, OLS showed an increase of about 14% from therapist 1. OLS showed fairly consistent results compared to the other algorithms for both metrics across therapists showing a deviation of 14% and 21% between therapist 1 and 2 respectively. For both metrics OLS performed better on the therapist 2 test dataset. IRL demonstrated the least desirable results for all tests. For both r^2 and MSE, the performance of IRL for therapist 2 decreased by half of its performance for therapist 1. It was only able to explain 41% and 26% of the variation in the output for therapist 1 and therapist 2 respectively. The results of the algorithms' predictions for both therapist test datasets were plotted in Figure 16. The plot for GPR shows the 95% confidence interval for its prediction in the gray shaded region. The full list of calculated values for r^2 and MSE were reported in Table 4.

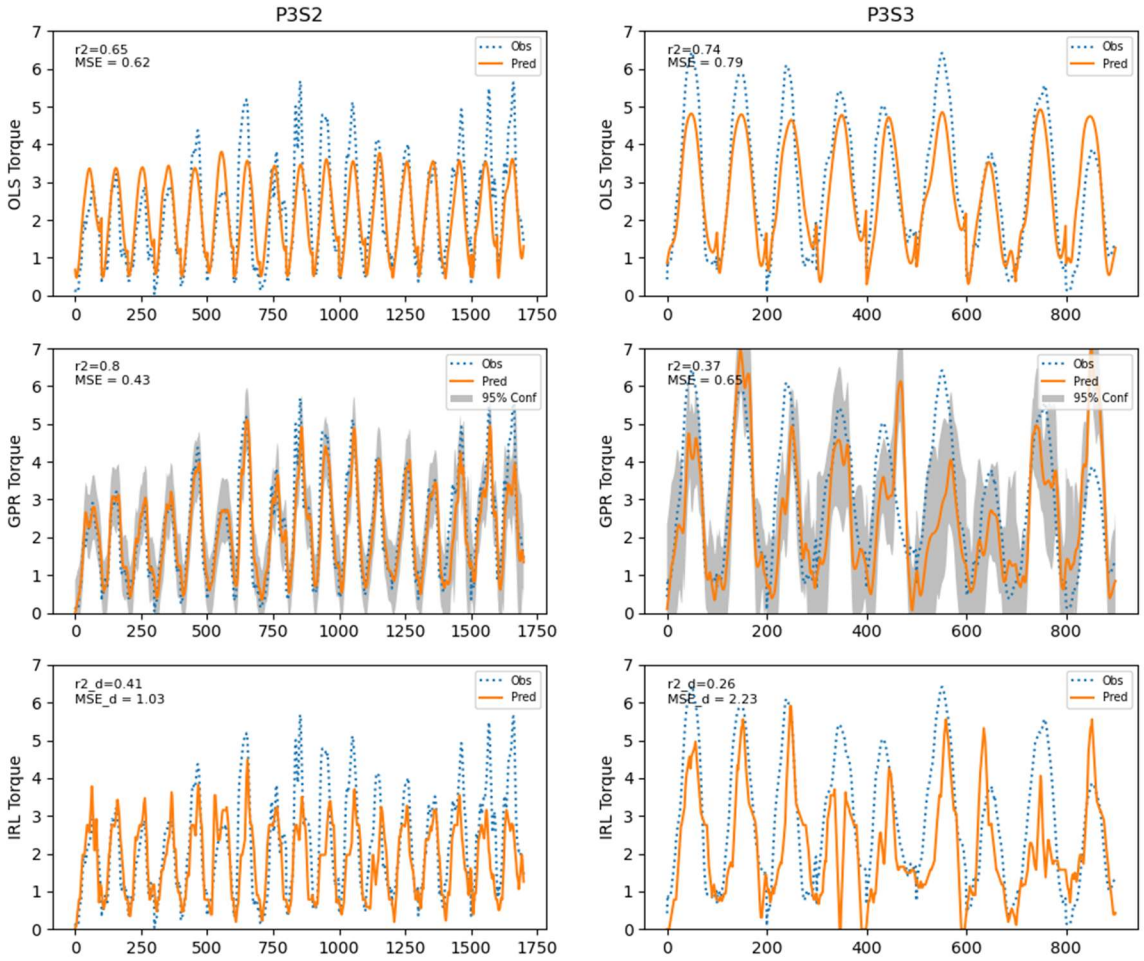

Figure 16: Algorithm Prediction Outcomes

Table 4
Standard Evaluation Metrics Results

	Therapist 1				Therapist 2			
Metric	OLS	GPR	IRL	[a]Best	OLS	GPR	IRL	[a]Best
r^2	0.65	0.8	0.41	GPR	0.74	0.37	0.26	OLS
MSE	0.62	0.43	1.03	GPR	0.79	0.65	2.23	GPR

Notes:
[a] Best refers to the algorithm that demonstrated the best performance for a given metric. For r^2 the best algorithm will have the highest reported value while the best algorithm for MSE will have the lowest reported value.

B. Analysis 2 Results: Emulating Therapist Assistance Characteristics

The therapist assistance characteristics $\boldsymbol{C}$ were calculated for all algorithm predictions over both therapist 1 and therapist 2 testing datasets. Table 5 provides the percent error in which the algorithms deviate from the observed therapist characteristic. The raw values for both the algorithm and therapist characteristics of assistance $\boldsymbol{C}$ can be found in APPENDIX A.

GPR was the only algorithm to maintain the smallest amount of deviation from the observed therapist characteristics across both the therapist 1 and therapist 2 sessions. This happened in both the $\bar{\tau}_{peak}$ and σ^2_{total} features were GPR significantly outperformed the other algorithms. In the σ^2_{total} feature, GPR obtained a deviation of 24.71% and 9.57% which is 18.97% and 26.43% better than the next closest algorithm; OLS. In the $\bar{\tau}_{peak}$ characteristic, GPR was able to obtain a margin of error of 6.67% and 5.01% for therapist 1 and therapist 2 respectively which is again followed by OLS with percent errors of 15.95% and 13.91%.

Although OLS and IRL tended to under-actuate, which resulted in their greater $\bar{\tau}_{peak}$ deviation, they outperformed GPR in matching the timing of the peak torque $\bar{t}_{peak}$ For therapist 1, IRL deviated by an average of 0.10% from the timing of demonstrated peak torque. This is in contrast to therapist 2's session where IRL had the largest deviation from the true mean peak time with 11.37% error. OLS's results were more consistent across therapist 1 and therapist 2 demonstrations with percent deviation if 6.55% and 1.15% respectively. In all other of the timing characteristics, $t_{start}, t_{end}, \Delta t_{sig}$, OLS showed the smallest deviation in the therapist 1 test dataset. In the therapist 2 test dataset, the minimum deviations for t_{end} and Δt_{sig} were produced by GPR with 2.33%

and 0.9% deviation respectively. IRL demonstrated the smallest deviation for t_{start} with a 17.64%. Across all therapists, the algorithms were more accurate in emulating the t_{end} characteristic than t_{start}.

No algorithm could sufficiently capture the peak variance feature (σ^2_{peak}). The minimum percent deviation throughout all trials was 44.12% and the next lowest being 77.27%. All but one of the results for this feature were caused by tight clustering of the peak variances when compared the how the therapists varied their peak actuation.

Table 5
Percent Error Deviation from Therapist Assistance Characteristics

	Therapist 1				Therapist 2			
Metric	OLS	GPR	IRL	[a]Best	OLS	GPR	IRL	[a]Best
$\bar{\tau}_{peak}$	15.95	6.67	20.71	GPR	13.91	5.01	31.91	GPR
$t_{sig_{start}}$	12.18	29.18	-26.7	OLS	40.51	36.5	-17.64	IRL
$t_{sig_{end}}$	-2.25	-2.44	5.79	OLS	-3.15	2.33	7.46	GPR
$\Delta\, t_{sig}$	-4.86	-8.17	11.71	OLS	-7.27	-0.9	9.82	GPR
$\bar{\mathrm{t}}_{peak}$	6.55	-7.87	-0.10	IRL	-1.15	-7.91	-11.37	OLS
σ^2_{peak}	98.04	44.12	82.35	GPR	81.82	-93.18	77.27	IRL
σ^2_{total}	43.68	24.71	52.3	GPR	36.3	9.57	59.41	GPR

Notes:
[a] Best refers to the algorithm that has the smallest absolute deviation from the observed therapist torque characteristic.

Figure 16 shows the predictions of each algorithm over the testing dataset. First, it is clear that OLS was able to match the timing and shape of the observed therapist assistance for both sessions. However, the peak magnitude for these predictions is mostly constant which is not indicative of the varying peak assistance demonstrated by the therapists. This is in contrast the other two algorithms that varied their peak torque that

reflects, but necessarily matches the magnitude of, the therapist demonstrations. It is also apparent that the GPR algorithm has a higher confidence in its predictions for therapist 1.

It should be noted that the results from the IRL algorithm were filtered using a modest linear filter to compensate for the fact that the predictions were discrete. The predictions from this model seem subject to a constant stochastic perturbation throughout both sessions. Additionally, more significant perturbations seem to invert the actuation behavior around select peaks. The most significant example of this occurs at i=350 for the therapist 2 session.

When the predictions are rescaled to fit within the domain of one stride, as seen in Figure 17, additional trends can be more easily observed. Primarily, the variance in predictions can be intuitively observed by the density of the prediction curves for each model. The most significant observation is that OLS has near zero variance in its predictions for therapist 1 and marginally more for therapist 2.

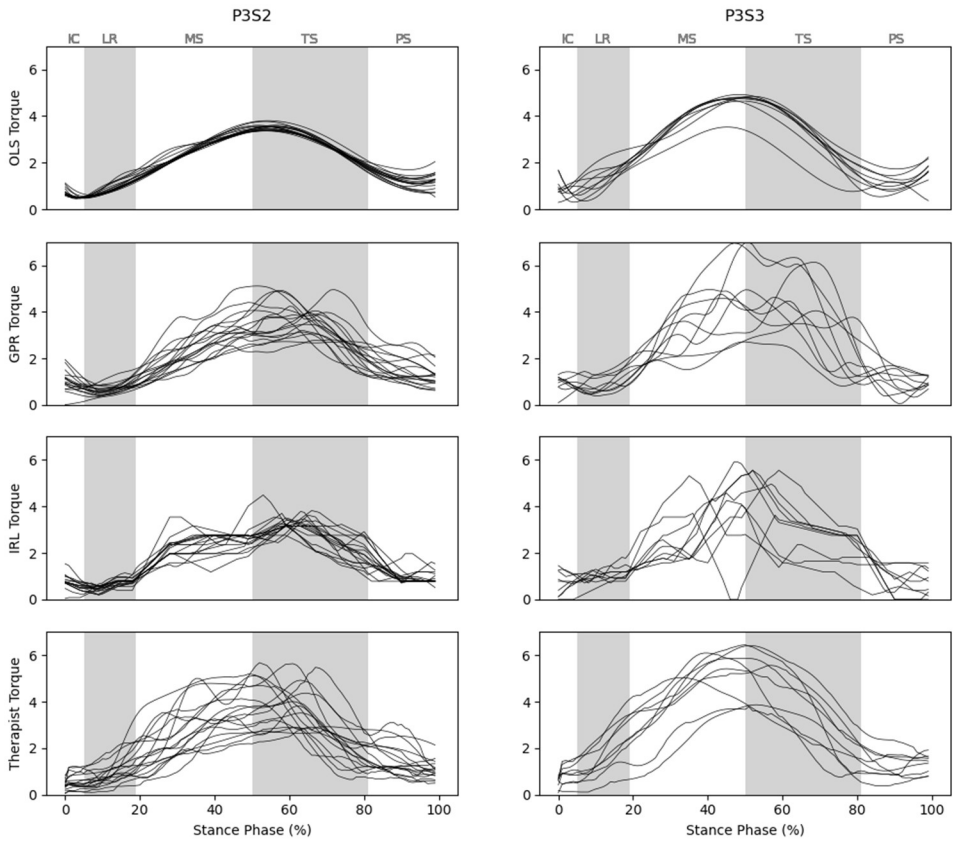

Figure 17: Algorithm Performance per Stride

C. Analysis 3 Results: Emulating Therapist Adaptations

To observe how well the algorithms emulated adaptation strategies, the assistance characteristics $\boldsymbol{C}$ were calculated for each stride. For each characteristic, the result for all algorithms and therapists were plotted over the course of both sessions. Next, a trendline was used to identify how the characteristic varied over the course of a session. Figure 18 provides an example of how the peak torque (top) varied for all algorithms over the course of a session, the calculated trendline (middle) that shows the adaptation of that characteristic as the session progresses and a bar graph (bottom) that compares the slope of each trendline. For the sake of brevity, the reported results for this analysis will only

show the slope of the trendlines for each characteristic while the full calculation for each characteristic can be found in .

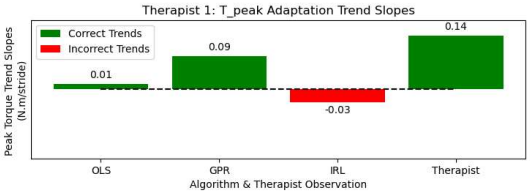

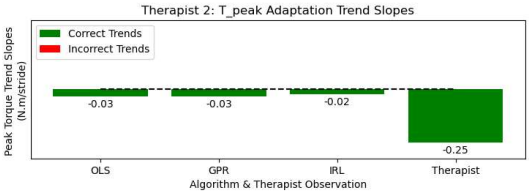

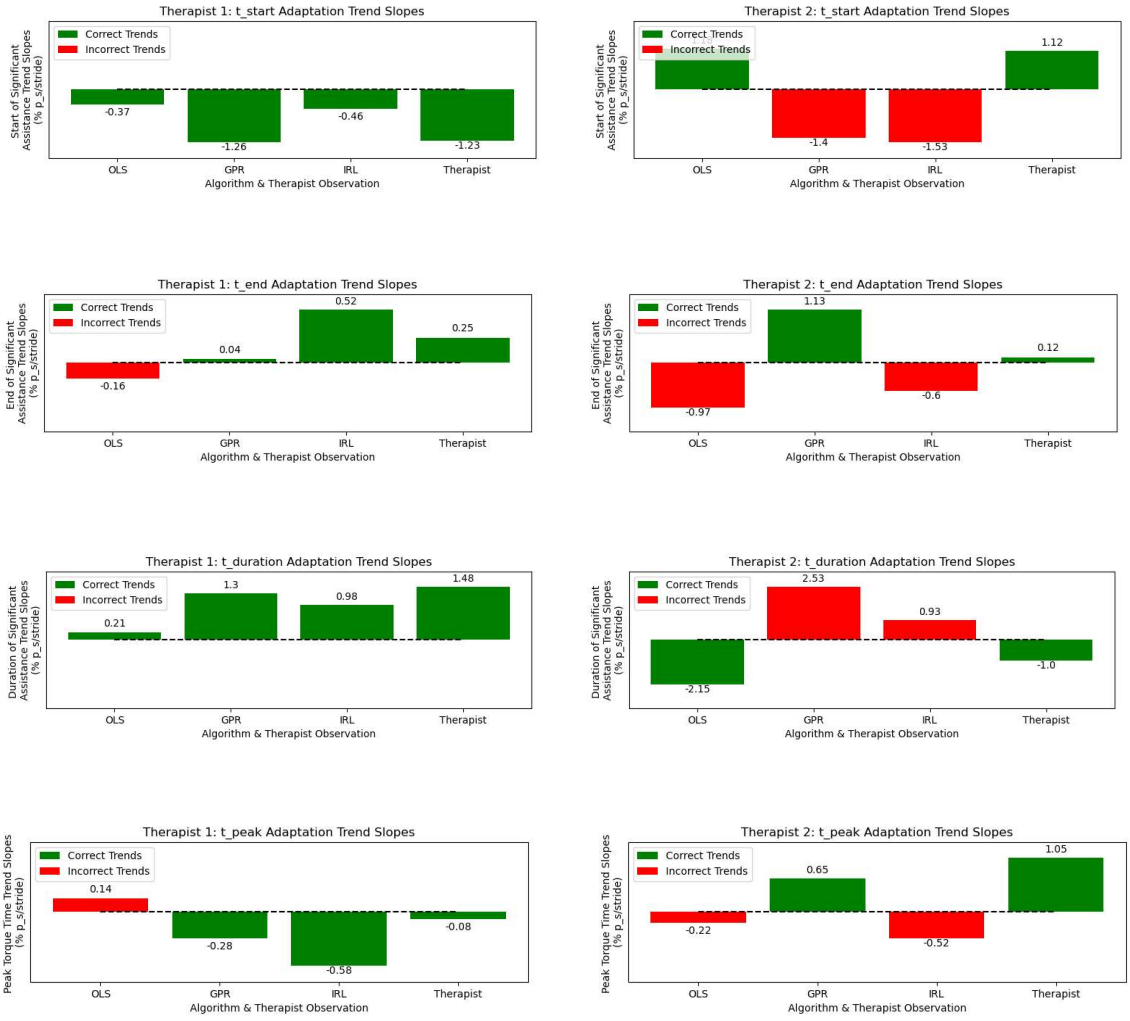

Figure 19. The full trend plots for these all characteristics can be found in Appendix B. Table 7 provides the full list of results for the calculated trend slopes of all algorithms and therapists for each session.

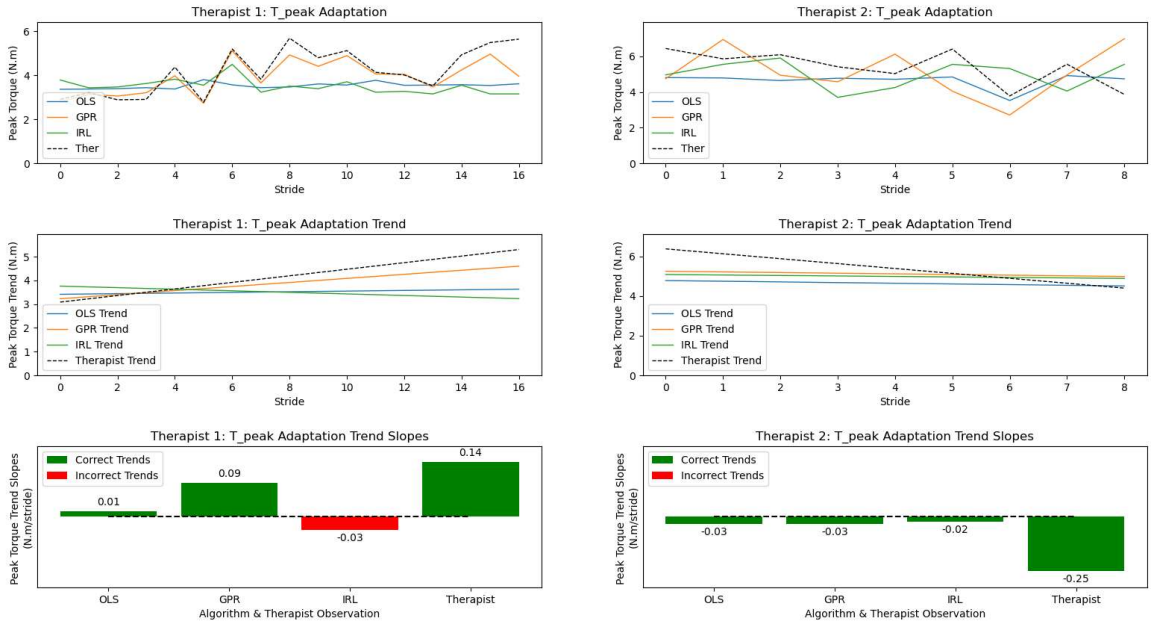

Figure 18: Adaption Trends for Peak Assistance

Therapist 1 and therapist 2 demonstrated inverse strategies for adapting to their assistive torque ($units: N.m$) over time. Therapist 1 increased the peak torque during each stride (m=0.14 $\frac{N.m}{stride}$) as the session went on while therapist 2 provided less maximum assistance as the session continued (m=-0.25 $\frac{N.m}{stride}$). For the session with therapist 1, GPR had the most similar trend (m=0.09). IRL demonstrated the incorrect trend (m=-0.03 $\frac{N.m}{stride}$) to what therapist 1 demonstrated. For the session with therapist 2, all algorithms correctly identified the negative trend and deviated from the true peak torque adaptation trend by approximately the same amount.

All algorithms were able to correctly identify the trend for varying the start of significant actuation $t_{start}(units: p_s)$ in the therapist session. However, GPR was the only algorithm to do so accurately with only a 2% deviation (m=-1.26 $\frac{p_s}{stride}$) from the

trend slope observed for therapist 1 (m=-1.23 $\frac{p_S}{stride}$). OLS (m=-0.37 $\frac{p_S}{stride}$) and IRL (m=-0.46 $\frac{p_S}{stride}$) deviated by 70% and 63% respectively. For therapist 2 (m=1.12 $\frac{p_S}{stride}$), only OLS (m=1.10 $\frac{p_S}{stride}$) was able to correctly identify the trend and was extremely accurate for with a deviation of 2%. Additionally, OLS was the only algorithm to correctly match the adaptation trends for both therapists.

For the $t_{end}(units: p_S)$ adaption trend, both therapists displayed the same adaptation trend but differed in the rate of adaptation with slopes m=0.25 $\frac{p_S}{stride}$ and m=0.12 $\frac{p_S}{stride}$ for therapists 1 and 2 respectively. GPR (m=0.04 $\frac{p_S}{stride}$ and m=1.13 $\frac{p_S}{stride}$) was able to identify the correct trend for both therapists while IRL (m=0.52 $\frac{p_S}{stride}$) was only able to identify the correct trend for therapist 2. OLS was able to identify neither trend correctly. No algorithm was able to significantly emulate the degree of adaptation.

For the Δt_{sig} $(units: p_S)$ adaption trend, the therapists displayed inverse adaptation trends with slopes m=1.49 $\frac{p_S}{stride}$ and m=-1.00 $\frac{p_S}{stride}$ for therapists 1 and 2 respectively. All algorithms were able to correctly identify the trend for therapist 1 while OLS was the only algorithm to correctly identify both. For therapist 1 GPR had the closest slope (m=1.3 $\frac{p_S}{stride}$) that was deviated 13% from the observed adaptation trend.

In regard to peak torque timing t_{peak} $(units: p_S)$, the therapists displayed inverse adaptation trends with slopes m=0.08 $\frac{p_S}{stride}$ and m=-1.05 $\frac{p_S}{stride}$ for therapists 1 and 2 respectively. The adaptation for therapist 1 is not significant and is therefore likely to have no adaptation strategy in when considering peak assistance time. Nonetheless, GPR

was the only algorithm to correctly identify both adaptation trends while IRL was only able to identify the trend for therapist 1.

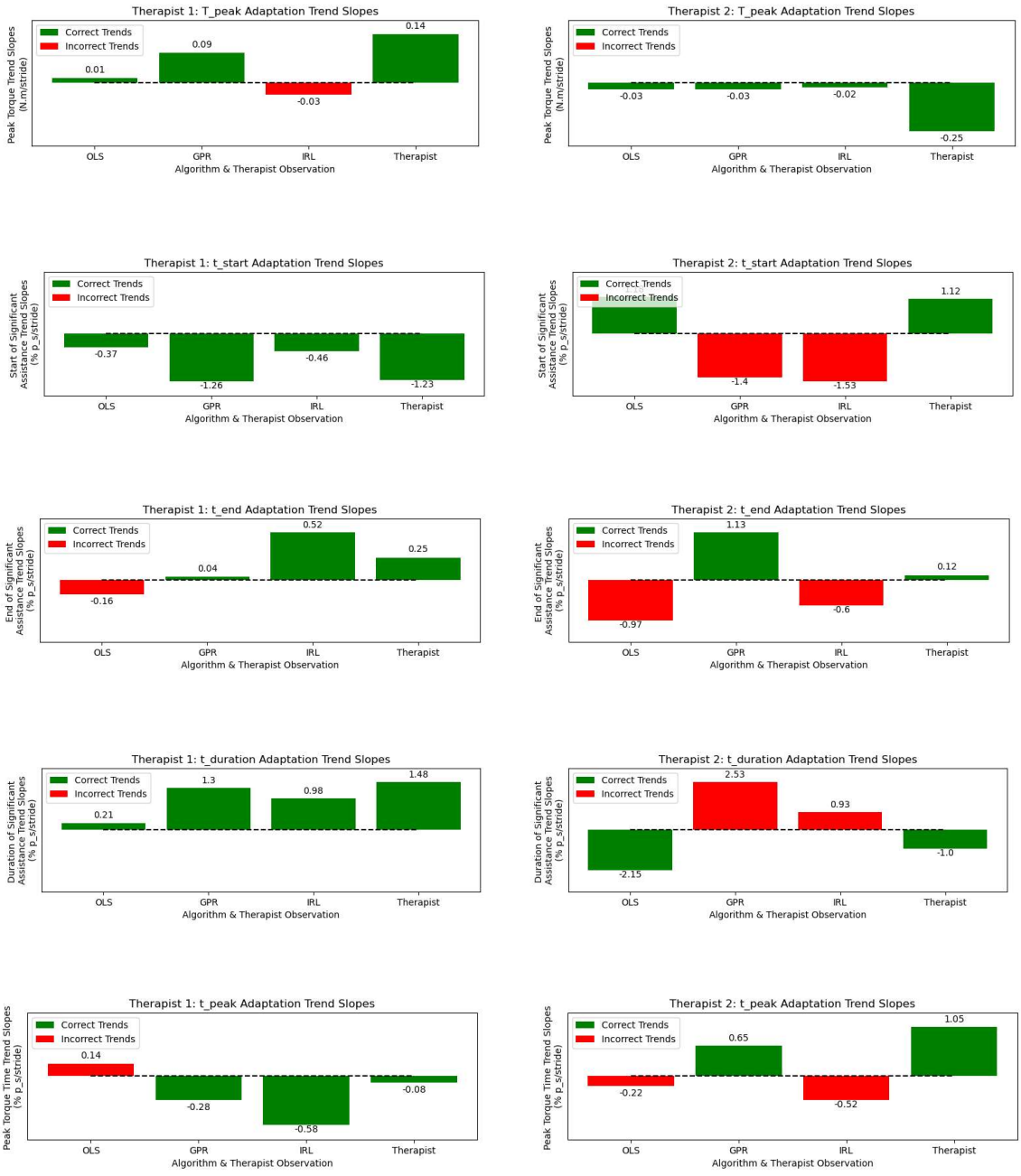

Figure 19: Adaption Trend Slopes for Characteristics of Assistance

Table 6
Correctly Identified Trends and Correlation of Therapist Strategies

Metric	OLS	GPR	IRL	[a]Correlation
τ_{peak}	Both	Both	T2	Inverse
t_{start}	Both	T1	T1	Inverse
t_{end}	Neither	Both	T1	Same
$\Delta\, t_{sig}$	Both	T1	T1	Inverse
t_{peak}	Neither	Both	T1	Inverse

Notes:
[a] Correlation refers to the relationship between the slopes of therapist 1 and therapist 2.
[b] T1 is shorthand for therapist 1 and T2 is shorthand for therapist 2

Table 7
Adaptation Trend Slopes

	Therapist 1				Therapist 2			
Metric	OLS	GPR	IRL	[a]Obs	OLS	GPR	IRL	[a]Obs
τ_{peak}	0.01	0.09	-0.03	0.14	-0.03	-0.03	-0.02	-0.25
t_{start}	-0.37	-1.26	-0.46	-1.23	1.10	-1.4	-1.53	1.12
t_{end}	-0.16	0.04	0.52	0.25	-0.97	1.13	-0.6	0.12
$\Delta\, t_{sig}$	0.21	1.3	0.98	1.49	-2.15	2.53	0.93	-1.00
t_{peak}	0.14	-0.28	-0.65	-0.08	-0.22	0.65	-0.50	1.05

Notes:
[a] Obs refers to the observed slope for therapist 1 and therapist 2

D. Inverse Reinforcement Learning's Recovered Reward Map

The recovered reward map from the MaxEnt IRL algorithm can be seen in Figure 20. This map displays the perceived therapist utility for putting the patient in a specific state during a particular phase. States colored yellow represent higher reward values while blue represents states with lower reward values. During the initial contact phase, there is little preference for any state over the others but as the patient progresses to mid stance the recovered reward map shows that the assistance becomes more critical. This can be seen by the differencing in the maximum reward value and the value of the

surrounding reward. During the initial contact, loading response and midstance phases the maximum agent utility is shown to be at $\theta_{hip} \in [7,11]$ and $\theta_{shank} \in [21,25]$. In the terminal stance phase, the state of maximum utility begins to move to greater hip displacement and less shank displacement with angles of at $\theta_{hip} \in [11,15]$ and $\theta_{shank} \in [12,15]$. Table 8 provides a full list of observations on the recovered reward map.

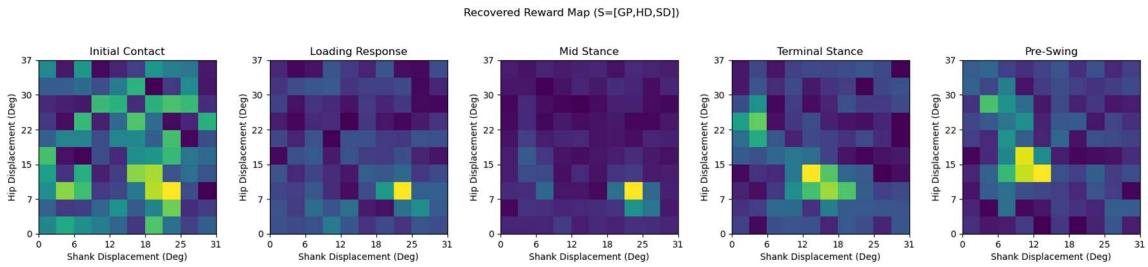

Figure 20: Recovered Reward Map

Table 8
Observed Therapist Reward

Phase	Observed
Initial Contact (IC)	Little preference for any state.
Loading Response (LR)	r_{max} at knee flexion 28° and 36°
Mid Stance (MS)	The mid-stance phase is observed to have the highest relative reward for r_{max}. Max utility begins to increase in the θ_{hip} dimension and decrease in the θ_{shank} dimension.
Terminal Stance (TS)	Relative significance of r_{max} decreases. Max utility continues to increase in the θ_{hip} dimension and decrease in the θ_{shank} dimension
Pre-Swing (PS)	Maximum utility continues to decrease in the θ_{hip} dimension.

8. DISCUSSION

This paper proposed the implementation and grounded evaluation of three machine learning algorithms to provide insight on methods for modeling therapists assistance. The approach to this problem was to develop methods to test performance of an algorithm's ability to emulate characteristics of assistance and therapist adaptation strategies. The results from this analysis and additional modeling considerations will be discussed in the following sections.

A. Information Loss from Unobserved Interactions

The first source of information loss that is observed in this research is caused by reducing the scope of the sensed features. Capturing the full range of interactions like therapist assistance can be extremely challenging due to their inherent complexity. Attempting to capture a wider scope often requires more sensing which can impede the training process and decrease the validity of the observed data. To address this tradeoff, a reduced model for considered therapist actions was created to decrease the sensing requirements for observing the system.

To justify this process of dimensionality reduction used in this research, it is helpful to discuss the set of all kinematic responses of the patient in response to a therapist. The patient responses can be described by a six degree of freedom mechanism in Figure # at a joint. Immediately, we can neglect considerations of all translations since this motion would result in shearing of the joint which is not productive for gait training. This leaves three axis of rotation that the therapist can responsibly actuate: extension and flexion, varus and valgus, and axial rotation axes.

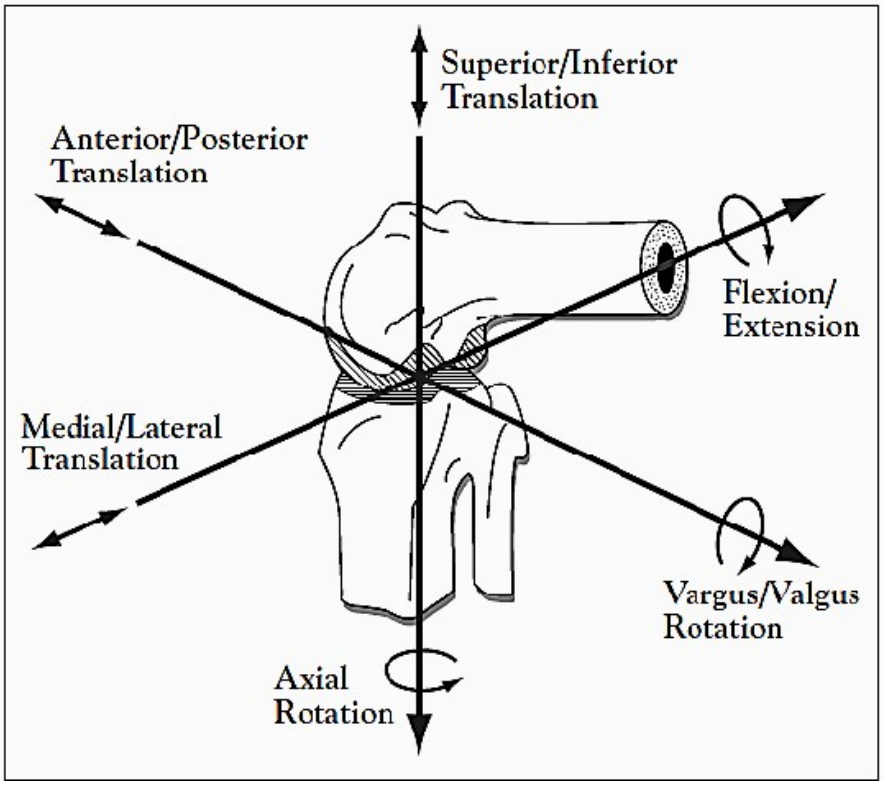

Figure 21: Joint Transformations [32]

The reduced interaction dynamics this research is obtained by considering only therapist assistance that is actionable by the one degree of freedom knee exoskeleton that this research is intended to control. Because the system is attached to the side of the knee, it can only actuate forces that contribute to rotating the limb around the knee extension and flexion rotation axis. Consequently, the only available action for the exoskeleton is apply to a torque around this same axis. This makes considerations of assistance about the varus and valgus axis and axial rotation axis not as immediately relevant for predicting assistance provided by the knee exoskeleton.

The simplified interaction model takes advantage of this by dividing the net force applied by the therapists into principal vector components that would contribute to only a

single one of the previously described axes of rotation. To further clarify this model, a two-dimensional representation of how the applied force by a therapist's hand is divided into these vector components is shown in Figure 22. In the image on the right, F_{EF} refers to the force that would cause rotation around the axis of extension and flexion rotation and F_{VV} around the axis of varus and valgus rotation.

However, the lower relevance of the other axes of rotation does not imply that that they contain no information that would contribute to improving the performance of the predictors to model the assistive force around the axis of knee extension and flexion. For example, assistance with lateral weight shifting is not considered in this model since this would cause rotation about the axis of varus and valgus rotation instead of extension and flexion. However, lateral weight shifting can be correlated to improper knee extension. This would make lateral forces, or a derivative of lateral forces, a possible candidate for being a predictor of assistance about the axis of knee extension and flexion rotation.

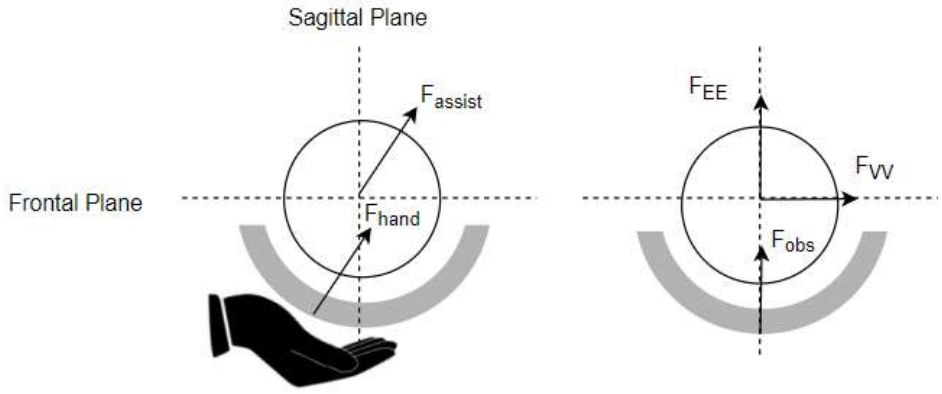

Figure 22: Reduced Interaction Model

Under the assumptions of this model, the data from the force sensors were able to generate a net force vector that describes the magnitude of the therapist's applied force and the angle at which the force was applied to both the thigh and shank by the therapist's hand or knee. Knowing the placement of the force sensor relative to the leg allows for the calculation of the net force vector F_{assist} that is applied to the thigh and shank and divided into the described vector components that actuate a single axis of rotation within a joint. Consequently, the assistive torque that is applied by the therapist around the axis of extension and flexion, F_{EF}, can be observed and used as training of the machine learning algorithms to predict the observed force.

iv. Assistance about the Axis of Varus and Valgus Rotation

Varus and valgus rotation refer to the rotation of the leg such that it moves within the frontal plane of the patient. Therapist can facilitate movements about this axis by providing a lateral force F_{VV} that is perpendicular to the force that the exoskeleton can

actuate F_{EF} by in Figure 22. As previously discussed, these forces have no immediate effect on what action the exoskeleton would take because they operate in different principal axes. However, this data could possibly provide access to features that can be extracted from this force.

v. Assistance about the Axis of Axial rotation

To control axial rotation, a therapist can grip the leg and rotate it about the length of the limb. The gripping action by the therapist can enter the observed forces F_{EF} by including the force necessary to maintain friction and the forces caused by the displacement of the sensors while rotating. Consider a therapist attempting to change the extension or flexion of a joint. In the left image of Figure 23, it can be seen how normal force of the hand F_N that is needed to grip the sensor can introduce a force vector in the direction of $F_{EF.}$ It follows that these forces can be mistakenly interpreted as therapist assistance. The right image shows a possible consequence of rotating the sensor. During this time, the top and bottom of the sensor would begin to experience sheer forces that would also be sensed as assistance in the sagittal plane.

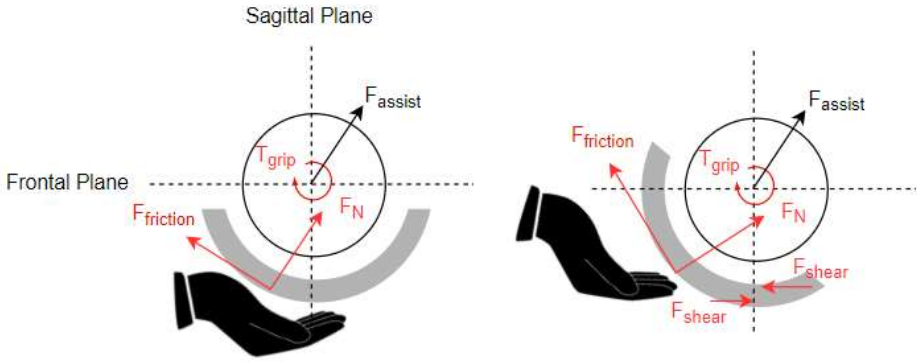

Figure 23: Effects of Axial Torques

vi. Opposition Forces

In addition to the forces applied to the front of the leg, therapists will often support the patient from the other side of the body similarly to Figure 24. This creates an opposition force that allows the therapist to maintain a higher level of control of the patient's leg by providing complementary forces that reduce the freely moving reactions of the patient. It can then be said that the resulting force that is intended by the therapist to facilitate proper knee flexion would be the difference between these two complementary forces.

Since sensors are not located behind the leg, this type of interaction was not observable by the data collection system. As a consequence, the opposition force vector is assumed to be zero and likely cause the observed assistance F_{obs} to be lower than the intended net force F_{EF} by the therapist that would actuate the intended rotation around the axis of extension and flexion.

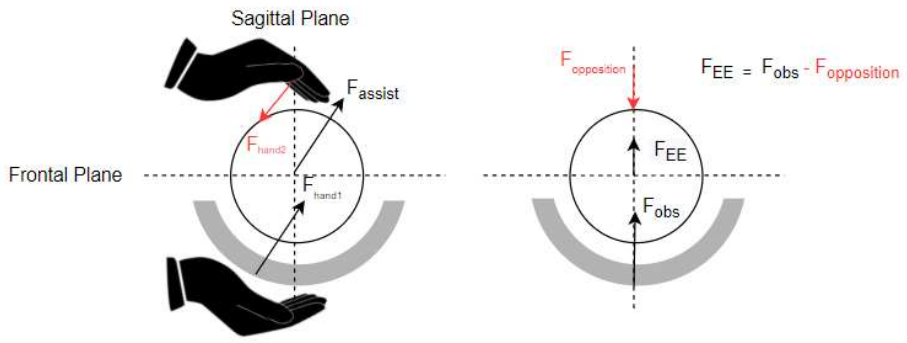

Figure 24: Effects of Opposition Forces

B. Information Loss from Dimensionality Reduction and Data Processing

The data collection system that was used for this research included three sensor sub-systems: two IMUs, four force sensors in a shoe, and 28 force sensors attached to the thigh and shank. The total number of raw values that were returned from all sensors was 33. This was then reduced to the final four selected training features: thigh and shank displacements, percent progression through the stance phase, and assistive torque around the knee.

For the IMU's dimensionality reduction, the additional reduction step from thigh and shank displacement to knee flexion was available but caused a significant decrease in correlation to the observed actions. Also, the relative rotation from zero displacement of the thigh and shank was chosen to increase accuracy and reliability of the data by reinitializing the reference position at the beginning of each lap, The trade-off for the lost absolute orientation information of the IMUs was deemed worth accounting for variation in initial conditions of attachment to the patient and drift over the long data collection sessions.

The initial GRFs data provided the ability to observe weight shifting and balancing characteristics. However, these are patient behaviors that are all addressed by lateral therapist assistance and are not relevant to the actuation of a one degree of freedom knee exoskeleton. However, percent progression through the gait phase can be extracted by interpolating the observed times of heel strike and toe up from 0 to 100 percent. Gait phase was assumed to be a good predictor since it defines what gait characteristics that the patient should be demonstrating given their progress through a step.

The final feature that was subject to information loss is the assistive torque applied about the axis of rotation of the knee. The primary motivation for choosing this feature was that it can be directly used as the control input for the knee-exoskeleton. The raw data contains 28 local force vectors applied to the thigh and leg which is not feasible to include the full dimensionality during training. Lucky, such high resolution is not necessary since all available response of the joint given a set of forces can be described in by the force components that cause rotations in axes described by Figure 21. As previously discussed, the exosuit is constrained to actuate around the axis of knee extension and rotation and therefore the other axis components would not be as relevant to this device's output.

In summation, a significant amount of information is lost by only considering forces that contribute to a net torque around the axis of knee extension and flexion. However, the excluded forces do not have as high of relevance in determining the magnitude of assistive knee torque for the exoskeleton as forces in the direction of F_{EF}. Also, it is likely that including these features would unreasonably increase computational

requirements of the learning algorithms and possibly decrease performance if the excluded features are not good predictors of the assistance we have defined as action for the exoskeleton. Also, there is loss of information through processing and interpretation of the raw sensor values that can be found in Figure 25 but the selected features were selected to optimize the tradeoff between tractability of training and the information retained.

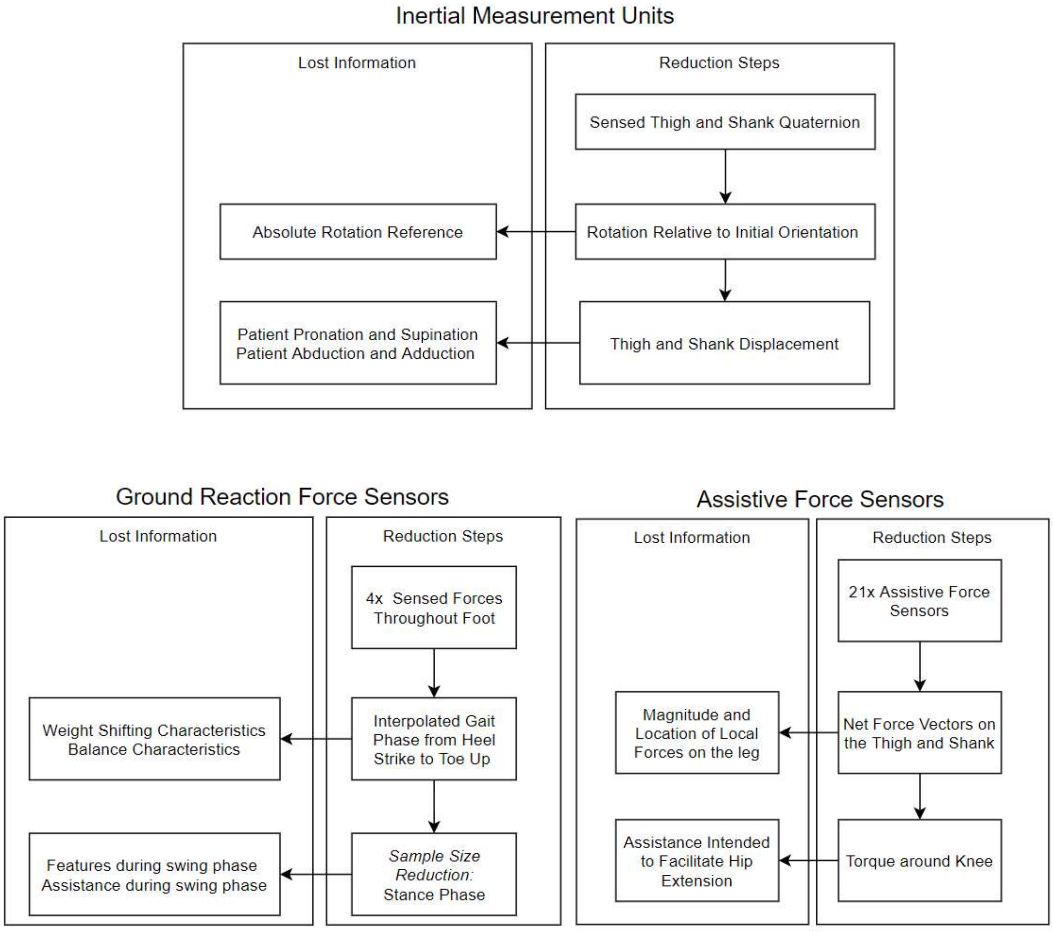

Figure 25: Dimensionality Reduction Steps and Losses

C. Sample Size for Therapist 1 and Therapist 2

An observation that arises from all tests is that algorithms generally performed better on the test dataset for therapist 1. This is likely to be caused by the disproportionate number of strides in the training sets for therapist 1 ($n_{strides} = 53$) and therapist ($n_{strides} = 24$) which manifested as a bias that favored emulating characteristics of therapist 1. The number of samples that were collected per therapist session were subject to patient fatigue and is therefore the most likely cause for this observation since therapist 2 data was collected after therapist 1.

There are a few methods to address this for future works. One method would be to truncate the data for therapist 1 to match therapist two thereby creating equal sample sizes. However, valid data was only able to be collected from one patient and reducing the number of strides in the training set would likely have negative consequences on performance. Another method would be to weight the training data. This would be a fairly simple method for accounting for this difference and will likely be implemented in a future iteration of this research.

D. Standard and Grounded Evaluation Insights

The standard methods for evaluation of predictive models, r^2 and MSE, showed that GPR was most likely the best algorithm to be used to predict the therapist assistance. However, the results from Analysis 2 showed that GPR was not the most desirable model in every dimension. For example, OLS was the best performing model for all features that concerned the period of significant actuation (t_{start}, t_{end} and Δt_{sig}) for therapist 1. Evaluating the algorithms with characteristics that relate to therapist assistance provides

analysis with a greater resolution. This is a significant result since it is likely that not all characteristics would be valued equally. Depending on the specific preferences of the occupational therapists, each one of the algorithms has the opportunity to be the optimal modeling method to choose. This is in contrast to if the decision were only based upon the standard evaluation metrics where GPR would be the objectively best algorithm to choose.

E. Ability to Emulate Assistance Characteristics

A significant observation is the poor performance of all algorithms in σ^2_{peak} and σ^2_{total} characteristics. This suggests that the therapists one of two possible conclusions. The first is that the variance in therapist assistance cannot be described by the observed states and that additional or alternative features would need to be used to increase accuracy for these characteristics. The second is that observations these characteristics are significantly more stochastic than the others. In other words, the therapist processes that dictate these characteristics are not as deterministic and cannot be predicted by the observed states in a meaningful way.

All algorithms were able to predict timing characteristics fairly well with the exception of t_{start}. OLS and GPR tended to start significant actuation a little too early. A possible cause for this behavior is that both of these algorithms fit a linear function that maps the states to prediction where the therapist is under no such constraint.

To simplify further discussion on relative performance of each algorithm, the number of times that each algorithm was rated either the best or worst was tallied and reported in Table 9 and plotted in Figure 26. OLS achieved least amount tallies for both

best and worst categories implying that it is a low-risk algorithm that limits the chance for optimal predictions. Although GPR and IRL both accumulated the same number of tallies for the worst rated algorithm, GPR did end up being the best algorithm to choose when all characteristics are weighted equally.

Table 9
Best and Worst Algorithm Tally

Algorithm	T1 # Best	T1 # Worst	T2 # Best	T2 # Worst	Total Best	Total Worst
OLS	2.0	1.0	0.0	3.0	2.0	4.0
GPR	3.0	3.0	4.0	2.0	7.0	5.0
IRL	2.0	3.0	3.0	2.0	5.0	5.0
Cumulative Best[a]	GPR	OLS	GPR	GPR; IRL	GPR	OLS

Notes: [a] Cumulative Best refers to either the most tallies for the "Best" category or the least number of tallies for the "Worst" category

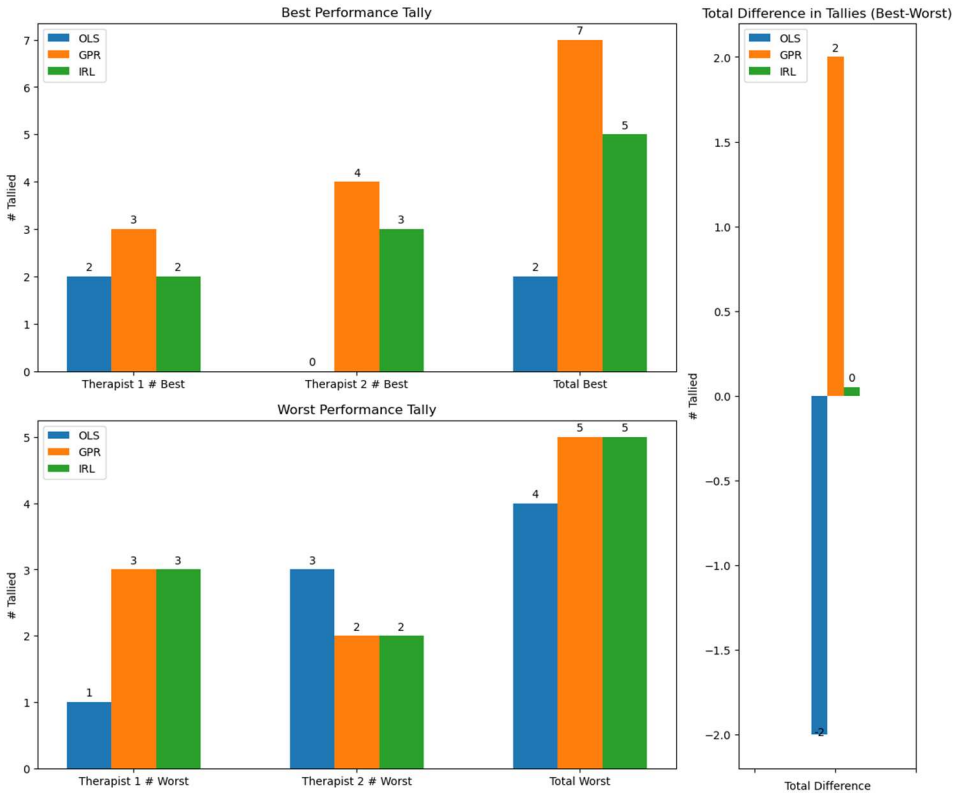

Figure 26: Best and Worst Performance Tallies

F. Ability to Emulate Therapist Strategies

GPR and IRL were able to correctly identify a trend for every feature. In IRL's case, four out of the five correctly identified trends were for therapist 1. This shows a strong bias to emulate therapist 1 and an inability to generalize its predictions strategies across multiple therapists. This is likely due to the difference in the number of samples in the training data. However, this bias is stronger for IRL than the others which suggest a higher sensitivity to the representation of different therapist characteristics and strategies in the training data. This bias could also explain the fact that IRL could not identify any trends for both therapists, but further analysis would be needed to confirm this.

OLS and GPR showed the equal capability to generalize their predictions to match to both therapist's adaptation trends. However, OLS was not able to correctly identify trends of either therapist in $t_{end}\ and\ t_{peak}$. Therefore, GPR can be said to be more accurate in identifying the adaptation trends while both GPR and OLS are equally capable of extending their adaptation trends to both therapists.

The most critical features that would be valued by a therapist would be the maximum assistance that is provided $\tau_{peak}\ and$ the time that the peak torque occurs t_{peak}. These features are important since they control the maximum actuation of the system. Therefore, they are tied to patient safety and presumed time that the patient needs the most assistance during the gait cycle. GPR was able to match the adaptation trends more accurately for τ_{peak} in session one than OLS. Also, GPR was able to correctly identify trends for both therapists in the t_{peak} feature where OLS was not. The fact that GPR was able to generalize its strategies for these critical features and the consistently high accuracy in matching the adaptation trend slope relative to other algorithms leads to the conclusion that GPR is likely the best algorithm to emulate therapist strategies.

9. CONCLUSION

The results of this research suggest that including a neurophysiological perspective into the evaluation of therapist modeling methods can provide additional insight into performance over standard methods. Mainly, an algorithm's ability to emulate therapist assistance depends on what characteristics or strategies are being evaluated. Observing this is simply not available when using standard evaluation metrics. Also, OLS and GPR showed the potential to emulate and generalize their presentation of

therapist strategies across therapists. While the results from standard evaluation metrics suggest that GPR is the most beneficial to choose, the grounded evaluation provides support for both OLS and GPR depending on the needs of the designer. In conclusion, the methods for evaluating algorithms in this way provides an opportunity to custom tailor the behavior of an algorithm to the needs of the platform.

A. Implications on Existing Control Methods

This research is intended to be an extension of existing impedance-based control methods that learn control parameters by observing therapist demonstrations during gait rehabilitation. Previous works like [33] use a Gaussian mixture model to learn the virtual impedance of a knee exoskeleton given the kinematic data of the patient. Results can also be extended to systems that use soft actuators like [34] since the control parameters only differs in calculation of the kinematic equations for assistive torque about the knee.

Implementing different learning methods in these contexts, as shown by the results of this research, have implications on the accuracy of mimicking assistance characteristics and the adaptation behaviors over the progression of the training session. Consequently, studies that control lower limb exoskeletons by observing therapist assistance like [33] and [34] have the opportunity to improve the performance of their exoskeletal systems by considering alternative modeling methods and additional perspectives during evaluation.

Specifically, the unique contribution that this research aims to add to these systems pertains to the level of insight included into the selection process of modeling methods for therapist assistance. This insight is gained by incorporating the grounded evaluation of algorithms that measures success in terms of emulating characteristics and

adaptation strategies of therapist assistance. This can be used as a framework when both considering new modeling methods and reevaluation of current methods for existing systems. Additionally, the data reported for the reviewed learning methods, OLS, GPR and IRL, can be directly used for comparison of performance to the methods used in other works. The final motivation for improving the modeling method for therapist assistance in this way is to improve the performance of these knee exoskeletons and eventually add to the quality of care of patients who stand to benefit from this technology.

B. Implications on the Field of Robotic Rehabilitation

A common issue of assistive rehabilitation devices is their lacking ability to incorporate the supervising therapist input into modifying the active assistance of the device. The therapist is instead asked only to provide the gait trajectories and initial motion primitives for the device while the controller is left to independently determine proper assistance and adapt to patient needs as they develop. This presents a missed opportunity to incorporate expert opinions as an input to the control system throughout the training session. As a result, this approach that promotes minimal therapist intervention is often viewed negatively by resident therapists which leads to poor acceptance of these devices into clinical settings [35].

This results research provides a method for supporting the use of different predictive algorithms by evaluating performance and behaviors in metrics that are more accessible to a supervising therapist than specifying standard performance criteria. This can allow the therapist a way to be more appropriately incorporated into the decision-

making process of selecting what controller should be considered to display the best performance.

There is also the novel opportunity to promote more active therapist involvement in a robotic assisted rehabilitation session. This opportunity comes from the finding that different assistance characteristics and strategies can be generated over the same dataset by implementing different modeling algorithms. Therefore, even with a low sample size, different impedance controller preferences and behaviors can be made available to the therapist so that they may select the one that most adequately matches the needs of the patient.

For example, the impedance controller could implement a predictive model generated by a different algorithm if the patient had trouble synchronizing with the system or if the assistance from the device was impeding therapist intervention. In this scenario, OLS predictions could be used instead of GPR, which generally performed better during evaluation, because OLS demonstrate highly consistent timing and peak assistance characteristics across strides. This behavior would be more predictable by the patient and therapist thereby improving the interaction if the context of the situation calls for it. In this scenario, a therapist would be enabled to more actively involved in assistance and contribute to the active preferences and behavior of the impedance controller itself.

Improvements to custom tailoring the assistance provided by a robotic device in this way can provide the necessary requirement to develop more effective and robust control systems. This in turn can affect the scope in which these devices are used. By generating devices that are able to generate the required behavior to compensate for

persistent motor deficits, in additional to functional therapy, assistive robotics could find their way out of the clinic and into the homes of the patients. Primarily, improvements to existing control methods could facilitate the use of assistive devices into ADLs [16] to improve the persistent quality of life for these patients in addition to their care during gait training.

C. Future Work

The implementation of the proposed algorithms was limited by several factors. Addressing some of these issues may be able to provide a more valid insight on the relative benefits and performance of the described evaluation metrics.

- Likely the most significant issue is that valid data was collected from one patient. Therefore, only an intra-patient evaluation can be conducted. This limits evaluation of the observation of how assistance characteristics and strategies would present themselves when faced with patients with different impairment levels and gait characteristics. Work that expands upon this research in the future should collect data from multiple patients and evaluate inter-patient effects.
- Including more machine learning algorithms would provide a better understanding of what approaches are best for emulating therapist assistance.
- Increasing the number of sensed features would allow the evaluation process to consider other therapist strategies.

REFERENCES

[1] D. Mozaffarian *et al.*, “Heart disease and stroke statistics-2016 update a report from the American Heart Association,” *Circulation*. 2016, doi: 10.1161/CIR.0000000000000350.

[2] J.-M. Belda-Lois *et al.*, “Rehabilitation of gait after stroke:a top down approach,” *J. Neuroeng. Rehabil.*, vol. 66, no. December, 2011.

[3] V. Dietz, “Interaction between central programs and afferent input in the control of posture and locomotion,” *J. Biomech.*, 1996, doi: 10.1016/0021-9290(95)00175-1.

[4] J.-M. Belda-Lois *et al.*, “Rehabilitation of Gait after Stroke: a Review Towards a Top-Down Approach,” *J. Neuroeng. Rehabil.*, vol. 8, no. 1, p. 66, 2011, doi: 10.1186/1743-0003-8-66.

[5] A. J. Bastian, “Understanding sensorimotor adaptation and learning for rehabilitation,” *Current Opinion in Neurology*. 2008, doi: 10.1097/WCO.0b013e328315a293.

[6] S. Lennon, “The Bobath concept: A critical review of the theoretical assumptions that guide physiotherapy practice in stroke rehabilitation,” *Physical Therapy Reviews*. 1996, doi: 10.1179/ptr.1996.1.1.35.

[7] S. M. Hatem *et al.*, “Rehabilitation of motor function after stroke: A multiple systematic review focused on techniques to stimulate upper extremity recovery,” *Front. Hum. Neurosci.*, 2016, doi: 10.3389/fnhum.2016.00442.

[8] J. Hidler, D. Nichols, M. Pelliccio, and K. Brady, “Advances in the understanding and treatment of stroke impairment using robotic devices,” *Topics in Stroke Rehabilitation*. 2005, doi: 10.1310/RYT5-62N4-CTVX-8JTE.

[9] D. J. Edwards, “On the understanding and development of modern physical neurorehabilitation methods: Robotics and non-invasive brain stimulation,” *Journal of NeuroEngineering and Rehabilitation*. 2009, doi: 10.1186/1743-0003-6-3.

[10] R. Gassert and V. Dietz, “Rehabilitation robots for the treatment of sensorimotor deficits: A neurophysiological perspective,” *J. Neuroeng. Rehabil.*, vol. 15, no. 1, pp. 1–15, 2018, doi: 10.1186/s12984-018-0383-x.

[11] R. P. S. Van Peppen, G. Kwakkel, S. Wood-Dauphinee, H. J. M. Hendriks, P. J. Van der Wees, and J. Dekker, “The impact of physical therapy on functional outcomes after stroke: What’s the evidence?,” *Clinical Rehabilitation*. 2004, doi: 10.1191/0269215504cr843oa.

[12] M. E. Dohring and J. J. Daly, “Automatic synchronization of functional electrical

stimulation and robotic assisted treadmill training," *IEEE Trans. Neural Syst. Rehabil. Eng.*, 2008, doi: 10.1109/TNSRE.2008.920081.

[13] J. A. M. Haarman, E. Maartens, H. Van Der Kooij, J. H. Buurke, J. Reenalda, and J. S. Rietman, "Manual physical balance assistance of therapists during gait training of stroke survivors: Characteristics and predicting the timing," *J. Neuroeng. Rehabil.*, vol. 14, no. 1, pp. 1–11, 2017, doi: 10.1186/s12984-017-0337-8.

[14] M. Mahdavian, S. Arzanpour, and E. J. Park, "Motion generation of a wearable hip exoskeleton robot using machine learning-based estimation of ground reaction forces and moments," *IEEE/ASME Int. Conf. Adv. Intell. Mechatronics, AIM*, vol. 2019-July, pp. 796–801, 2019, doi: 10.1109/AIM.2019.8868759.

[15] J. A. Galvez, A. Budovitch, S. J. Harkema, and D. J. Reinkensmeyer, "Trainer variability during step training after spinal cord injury: Implications for robotic gait-training device design," *J. Rehabil. Res. Dev.*, vol. 48, no. 2, pp. 147–160, 2011, doi: 10.1682/JRRD.2010.04.0067.

[16] C. Glackin *et al.*, "Learning gait by therapist demonstration for natural-like walking with the CORBYS powered orthosis," *IEEE Int. Conf. Intell. Robot. Syst.*, vol. 2015-Decem, pp. 5605–5610, 2015, doi: 10.1109/IROS.2015.7354172.

[17] W. Zhang, M. Tomizuka, and N. Byl, "A Wireless Human Motion Monitoring System for Smart Rehabilitation," *J. Dyn. Syst. Meas. Control. Trans. ASME*, vol. 138, no. 11, Nov. 2016, doi: 10.1115/1.4033949.

[18] C. Sammut, "Behavioral Cloning," in *Encyclopedia of Machine Learning*, C. Sammut and G. I. Webb, Eds. Boston, MA: Springer US, 2010, pp. 93–97.

[19] P. Abbeel and A. Y. Ng, "Apprenticeship learning via inverse reinforcement learning," *Proceedings, Twenty-First Int. Conf. Mach. Learn. ICML 2004*, pp. 1–8, 2004, doi: 10.1145/1015330.1015430.

[20] S. Shalev-Shwartz and S. Ben-David, *Understanding Machine Learning: From Theory to Algorithms*. New York: Cambridge University Press, 2013.

[21] J. Silvério, Y. Huang, L. Rozo, and D. G. Caldwell, "An Uncertainty-Aware Minimal Intervention Control Strategy Learned from Demonstrations," in *IEEE International Conference on Intelligent Robots and Systems*, Oct. 2018, pp. 6065–6071, doi: 10.1109/IROS.2018.8594220.

[22] B. D. Ziebart, A. Maas, J. A. Bagnell, and A. K. Dey, "Maximum entropy inverse reinforcement learning," in *Proceedings of the National Conference on Artificial Intelligence*, 2008, vol. 3, pp. 1433–1438.

[23] "Ordinary Least-Squares (OLS) Regression."

https://vulstats.ucsd.edu/notes/bivariate-ols.html (accessed Apr. 01, 2021).

[24] C. Anderson and R. E. Schumacker, “A Comparison of Five Robust Regression Methods With Ordinary Least Squares Regression: Relative Efficiency, Bias, and Test of the Null Hypothesis,” *Underst. Stat.*, 2003, doi: 10.1207/s15328031us0202_01.

[25] G. Hutcheson and N. Sofroniou, *The Multivariate Social Scientist*. 1999.

[26] C. . Rasmussen and C. Williams, *Gaussian Processes in Machine Learning*. Heidelberg: MIT Press, 2006.

[27] J. Görtler, R. Kehlbeck, and O. Deussen, “A Visual Exploration of Gaussian Processes.” .

[28] D. K. Duvenaud, “Automatic Model Construction with Gaussian Processes,” *Https://Github.Com/Duvenaud/Phd-Thesis*, no. June, p. 144, 2014.

[29] A. Ng and S. Russell, “Algorithms for inverse reinforcement learning,” *Proc. Seventeenth Int. Conf. Mach. Learn.*, 2000.

[30] E. Olariu, K. Cadwell, E. Hancock, D. Trueman, and H. Chevrou-Severac, “Current recommendations on the estimation of transition probabilities in Markov cohort models for use in health care decision-making: a targeted literature review,” *Clin. Outcomes Res.*, vol. Volume 9, pp. 537–546, Sep. 2017, doi: 10.2147/CEOR.S135445.

[31] T. Stöckel, R. Jacksteit, M. Behrens, R. Skripitz, R. Bader, and A. Mau-Moeller, “The mental representation of the human gait in young and older adults,” *Front. Psychol.*, vol. 6, no. 1, p. 943, 2015.

[32] S. Fathy and M. El Messiry, “Study of the Effect of Cyclic Stress on the Mechanical Properties of Braided Anterior Cruciate Ligament (ACL),” *J. Text. Sci. Eng.*, vol. 06, no. 02, 2016, doi: 10.4172/2165-8064.1000252.

[33] P. T. Chinimilli, Z. Qiao, S. M. Rezayat Sorkhabadi, V. Jhawar, I. H. Fong, and W. Zhang, “Automatic virtual impedance adaptation of a knee exoskeleton for personalized walking assistance,” *Rob. Auton. Syst.*, vol. 114, pp. 66–76, Apr. 2019, doi: 10.1016/j.robot.2019.01.013.

[34] S. Sridar *et al.*, “Evaluating Immediate Benefits of Assisting Knee Extension With a Soft Inflatable Exosuit,” *IEEE Trans. Med. Robot. Bionics*, vol. 2, no. 2, pp. 216–225, Apr. 2020, doi: 10.1109/tmrb.2020.2988305.

[35] J. Fong, H. Rouhani, and M. Tavakoli, “A Therapist-Taught Robotic System for Assistance During Gait Therapy Targeting Foot Drop,” *IEEE Robot. Autom. Lett.*, vol. 4, no. 2, pp. 407–413, 2019, doi: 10.1109/LRA.2018.2890674Y.

APPENDIX A

RAW CHARACTERISTICS OF ASSISTANCE VALUES

Table 10
Algorithm and Therapist Assistance Characteristics

	Therapist 1				Therapist 2			
Metric	OLS	GPR	IRL	Therapist	OLS	GPR	IRL	Therapist
$\bar{\tau}_{peak}$	3.53	3.92	3.33	4.2	4.64	5.12	3.67	5.39
$t_{sig_{start}}$	12.76	10.29	18.41	14.53	4.89	5.22	9.67	8.22
$t_{sig_{end}}$	96.53	96.71	88.94	94.41	98.33	93.11	88.22	95.33
$\Delta\, t_{sig}$	83.76	86.41	70.53	79.88	93.44	87.89	78.56	87.11
$\bar{\mathrm{t}}_{peak}$	54.47	62.88	58.35	58.29	48.22	51.44	53.09	47.67
σ^2_{peak}	0.02	0.57	0.18	1.02	0.16	1.7	0.2	0.88
σ^2_{total}	0.98	1.31	0.83	1.74	1.93	2.74	1.23	3.03

APPENDIX B

FULL ADAPTATION TREND PLOTS

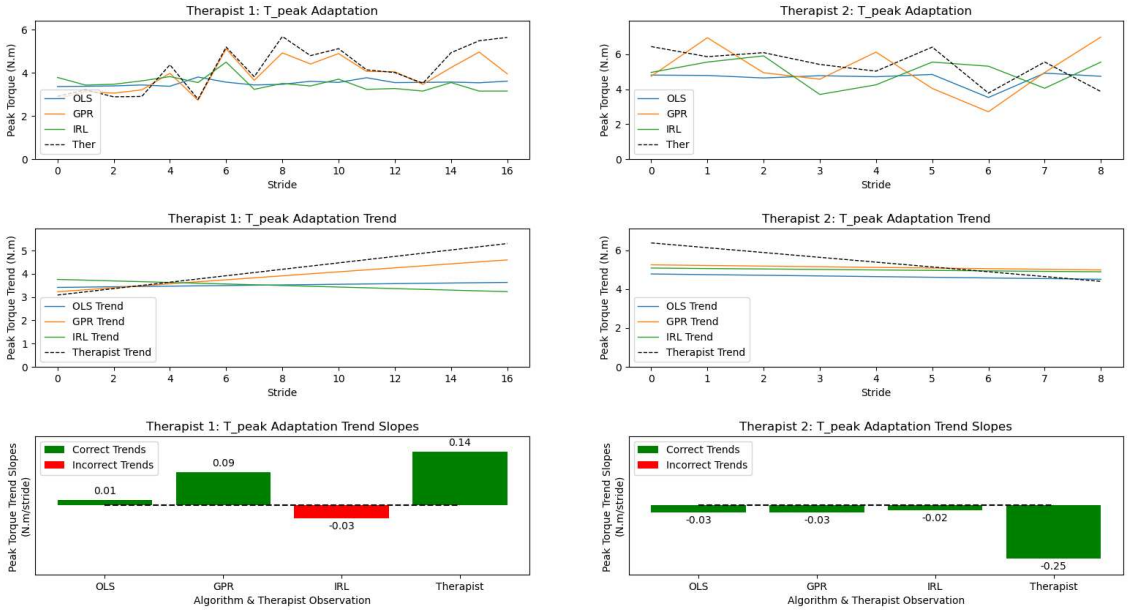

Figure 27: Full Adaptation Trend Plot for Peak Torque

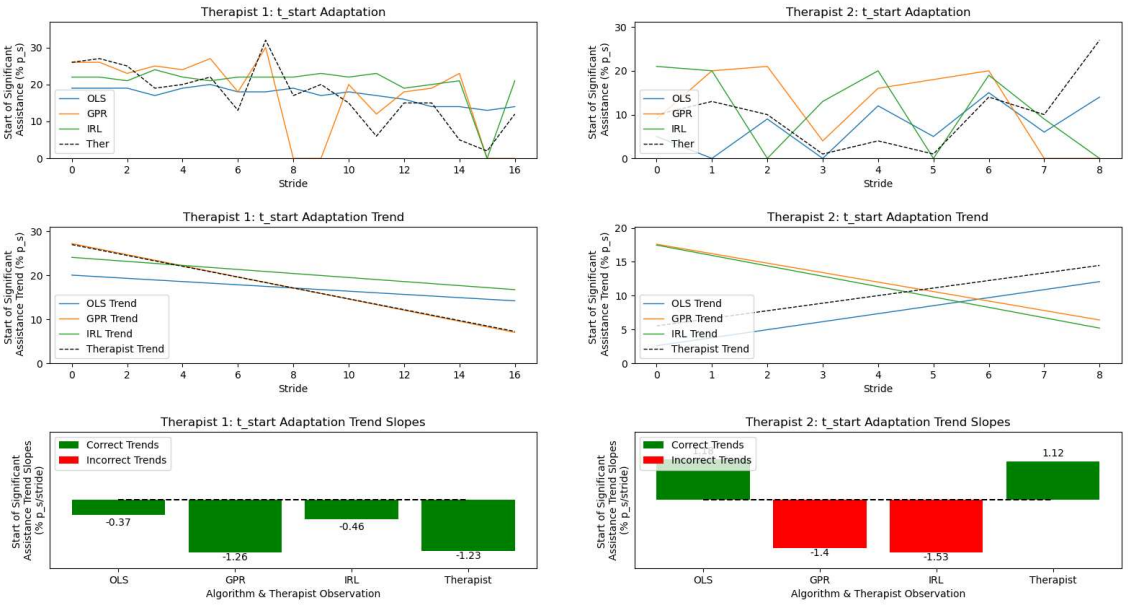

Figure 28: Full Adaptation Trend Plot for Start Time of Significant Actuation

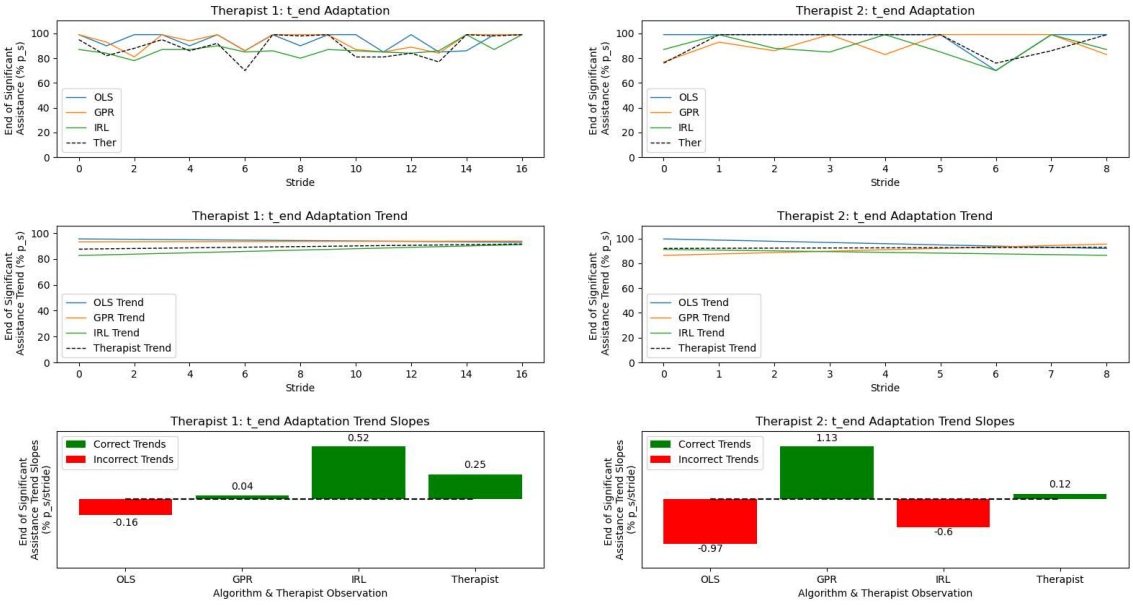

Figure 29: Full Adaptation Trend Plot for End Time of Significant Actuation

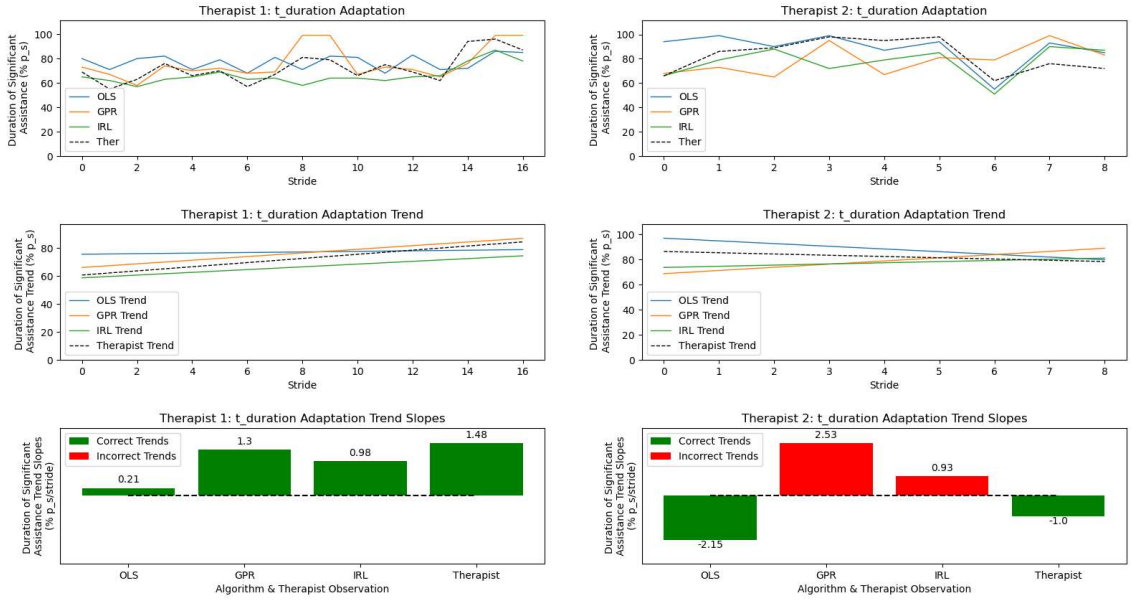

Figure 30: Full Adaptation Trend Plot for Duration of Significant Actuation

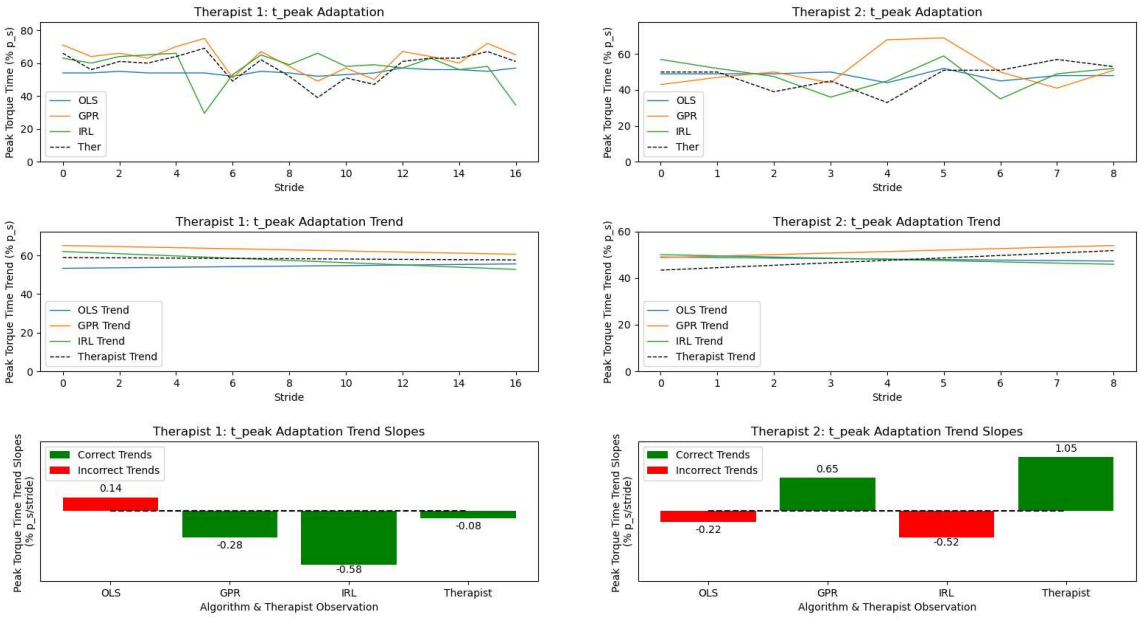

Figure 31: Full Adaptation Trend Plot for Peak Actuation Time